

Properties and Foaming Behaviour of Thermoplastic Olefin
Blends Based on Linear and Branched Polypropylene

by

TARA J. McCALLUM

A thesis submitted to the Department of Chemical Engineering
in conformity of the requirements for
the degree of Master of Science (Engineering)

Queen's University
Kingston, Ontario, Canada
September 2007

Copyright © Tara J. McCallum, 2007

Abstract

The recent commercial availability of branched polypropylenes (PPs) combined with the advent of single-site metallocene catalysts has ignited interest in thermoplastic polyolefin blends (TPOs) with controlled melt strength. These blends have potential applications in a variety of industries including foam processing and extrusion foaming.

The main objective of the thesis is to provide a detailed investigation on the rheological, morphological, thermal, mechanical and foaming properties of isotactic polypropylene / high melt strength branched polypropylene homopolymer blends, and of thermoplastic olefin blends using these polypropylenes as matrices.

Initial research on the polypropylene blends consisted of a linear high melt flow rate PP and two branched PPs with different melt flow rates. Blends containing branched PPs display evidence of miscibility in the melt state and exhibit high melt elasticity together with significant strain hardening in extensional deformation while retaining good flow properties. Of the two blend systems examined, the blends containing linear and branched PPs with similar melt flow rates have better mechanical properties, higher crystallization temperatures, and higher crystallinities.

An investigation into the mechanical, thermal, rheological, morphological, and microcellular foaming behaviour of TPO blends consisting of a blended matrix of linear and branched PP with a dispersed phase of an ethylene-octene copolymer was performed. Blends containing branched PP showed improved stiffness and flexural properties. Given that the morphology and interfacial tension of the blends remain virtually unaffected, these improvements are attributed to the increased crystallinity in the presence of a

branched component with higher molecular weight. Varying the amount of branched PP into linear PP during foaming experiments in a batch foaming simulation apparatus caused slower cell growth rates and decreased cell densities, while TPO foams showed polydispersity in the cell sizes, possibly due to the different foaming characteristics of the immiscible components.

The addition of talc to TPO blends aims at improving the stiffness and dimensional stability of the material, while lowering material costs. Blends of linear and branched PP with an ethylene-octene copolymer dispersed phase and uncalcinated talc showed similar trends, as well as an expected drop in the elongation at break. There was an increase in the viscosity and crystallinity of the blends, and optimum gains were seen in blends containing 20 wt% branched PP. Increasing the levels of branched PP did not significantly affect the bubble growth rate, or the final cell density during foaming experiments.

Co-Authorship

This thesis contains one chapter that presents results that have been published in the form of an original paper. The complete citation for this paper and the chapters in which they appear are provided below:

Chapter 3: T.J. McCallum, M. Kontopoulou, C.B. Park, E.B. Muliawan and S.G. Hatzikiriakos, *Polymer Eng Sci*, 47, 1133 (2007).

This paper was co-authored by Dr. Marianna Kontopoulou and Dr. Chul B. Park. This paper was also co-authored by Edward B. Muliwan and Dr. Savvas G. Hatzikiriakos as they conducted extensional rheology measurements and its subsequent analysis. All of the remaining work and manuscript preparation was performed by the author. The manuscript was reviewed by Dr. Marianna Kontopoulou and Dr. Chul B. Park prior to submission for publication.

Acknowledgements

First and foremost, I would like to thank my supervisor, Dr. Marianna Kontopoulou for the opportunity to continue my studies as a graduate student here at Queen's. Her guidance and support made this project both interesting and rewarding. I would also like to thank my co-supervisor, Dr. Chul Park, for his knowledge and encouragement, as well as colourful discussions about my future. I greatly appreciated the time he took out of his busy schedule for our one-on-one chats.

I am greatly indebted to my family, especially my parents, Hugh and Fran McCallum, and my two big brothers, Aron and Kyle. Thanks for all the love and support you gave me, as well as the bumps and bruises. Without these experiences, I would not have been the same person, and this endeavour could not have been possible. To my friends, lab-mates, team-mates, and the chemical engineering staff, thanks for all the laughs and unforgettable moments. You have all made my stay in Kingston a truly enjoyable experience. A special thanks to Adam St. John for anything and everything.

Lastly, this work could not have been done without the financial support from AUTO 21 Network of Centres of Excellence and Decoma International, as well as the donation of polymer resins from Basell. I would also like to thank Charlie Cooney for his expertise with SEM, Edward Muliawan and Prof. Savas Hatzikiriakos for their assistance with extensional rheology, Mohammad Hasan, Ryan Kim and Anson Wong for their aid with solubility measurements and foaming experiments, and Prof. M. Bousmina and Dr. Steve Poulliot for their help with GPC measurements.

Table of Contents

<i>Abstract</i>	i
<i>Co-Authorship</i>	iii
<i>Acknowledgements</i>	iv
<i>List of Tables</i>	ix
<i>List of Figures</i>	x
<i>Nomenclature</i>	xiii
CHAPTER 1 Introduction	1
1.1 Polyolefin-Based Polymers in Automotive Applications	1
1.2 Linear and Branched Polypropylene	2
1.3 Polypropylene-Based Blends	3
1.4 Foaming of Polyolefins	4
1.5 Objectives and Outline	5
1.6 References	6
CHAPTER 2 Literature Review	7
2.1 Polymer Blends	7
2.1.1 Determination of Polymer Miscibility	8
2.2 Morphology of Polymer Blends	10
2.2.1 Droplet Geometry	11
2.2.2 Droplet Breakup and Coalescence	11

2.2.3	<i>Interfacial Tension</i>	13
2.3	Relating Morphology to Rheology: The Palierne Emulsion Model	14
2.4	Foaming Theory	17
2.4.1	<i>Foaming Mechanism – Nucleation, Cell Growth and Coalescence</i>	18
2.4.2	<i>Cell Growth and Coalescence</i>	19
2.4.3	<i>Foam Processing</i>	20
2.4.4	<i>Polyolefin Foams</i>	21
2.5	References	24
	<i>CHAPTER 3 The Rheological and Physical Properties of Linear and Branched Polypropylene Blends</i>	28
3.1	Introduction	28
3.2	Experimental	30
3.2.1	<i>Materials</i>	30
3.2.2	<i>Blend Preparation</i>	31
3.2.3	<i>Rheological Characterization</i>	31
3.2.4	<i>Thermal Properties</i>	33
3.2.5	<i>Mechanical Properties</i>	33
3.3	Results and Discussion	34
3.3.1	<i>Oscillatory Shear Rheology</i>	34
3.3.2	<i>Steady Shear Rheology</i>	42
3.3.3	<i>Extensional Rheology</i>	44
3.3.4	<i>Thermal Properties</i>	47
3.3.5	<i>Mechanical Properties</i>	49
3.4	Conclusions	51

3.5	References	51
------------	-------------------	----

CHAPTER 4 Morphology, Properties and Foaming Characteristics of TPOs Based on Blends of Linear and Branched Polypropylene _____ 54

4.1	Introduction	54
------------	---------------------	----

4.2	Experimental	55
------------	---------------------	----

4.2.1	<i>Materials</i>	55
-------	------------------	----

4.2.2	<i>Blend Preparation</i>	56
-------	--------------------------	----

4.2.3	<i>Rheological Characterization</i>	56
-------	-------------------------------------	----

4.2.4	<i>Scanning Electron Microscopy</i>	57
-------	-------------------------------------	----

4.2.5	<i>Thermal Properties</i>	57
-------	---------------------------	----

4.2.6	<i>Mechanical Properties</i>	57
-------	------------------------------	----

4.2.7	<i>Batch Foaming Experiments</i>	58
-------	----------------------------------	----

4.3	Results	60
------------	----------------	----

4.3.1	<i>Blend Morphology</i>	60
-------	-------------------------	----

4.3.2	<i>Mechanical Properties</i>	64
-------	------------------------------	----

4.3.3	<i>Batch Foaming Experiments</i>	67
-------	----------------------------------	----

4.4	Conclusions	75
------------	--------------------	----

4.5	References	76
------------	-------------------	----

CHAPTER 5 Physical Properties and Foaming of Talc-Filled TPOs Based on Blends of Linear and Branched Polypropylene _____ 78

5.1	Introduction	78
------------	---------------------	----

5.2	Experimental	80
------------	---------------------	----

5.2.1	<i>Materials</i>	80
-------	------------------	----

5.2.2	<i>Blend Preparation</i>	81
5.2.3	<i>Rheological Characterization</i>	81
5.2.4	<i>Thermal Properties</i>	82
5.2.5	<i>Scanning Electron Microscopy</i>	82
5.2.6	<i>Mechanical Properties</i>	82
5.2.7	<i>Batch Foaming Experiments</i>	82
5.3	Results and Discussion	83
5.3.1	<i>Rheological Characterization</i>	83
5.3.2	<i>Mechanical and Thermal Properties</i>	85
5.3.3	<i>Batch Foaming Experiments</i>	91
5.4	Conclusions	93
5.5	References	93
	CHAPTER 6 Conclusions and Recommendations	95
6.1	Conclusions	95
6.2	Recommendations for Future Work	96

List of Tables

Table 3.1. <i>Material Properties.</i>	31
Table 3.2. <i>Cross and power law model parameters for LPP35/BPP30 and LPP35/BPP2.5 blends.</i>	38
Table 3.3. <i>Thermal and tensile properties for LPP35/BPP30 and LPP35/BPP2.5 blends.</i>	48
Table 5.1. <i>Thermal properties of compounded TPOs (both with and without 10 wt% talc) with varying levels of Branched PP.</i>	89

List of Figures

Figure 2.1. <i>Diagram of the microcellular foaming process [64].</i> _____	21
Figure 3.1. <i>(a) Complex viscosities, η^* and (b) elastic moduli, G', as a function of frequency, ω, for LPP35/BPP30 blends at 180°C.</i> _____	35
Figure 3.2. <i>(a) Complex viscosities, η^* and (b) elastic moduli, G', as a function of frequency, ω, for LPP35/BPP2.5 blends at 210 °C.</i> _____	36
Figure 3.3. <i>Zero shear viscosity of LPP35/BPP2.5 and LPP35/BPP30 blends at 210°C and 180°C respectively. Solid lines denote the log-additivity rule of viscosity.</i> _____	39
Figure 3.4. <i>Cole-cole plots of (a) LPP35/BPP30 blends at 180°C, (b) LPP35/BPP2.5 blends at 210 °C.</i> _____	40
Figure 3.5. <i>Weighted relaxation spectra of LPP35/BPP30 blends at 180°C.</i> _____	42
Figure 3.6. <i>Combined shear and complex viscosities as a function of shear rate or frequency at 210°C; (a) LPP35/BPP30 blends; (b) LPP35/BPP2.5 blends. Open symbols denote capillary data, whereas closed symbols represent oscillatory data.</i> _____	43
Figure 3.7. <i>Extensional stress growth coefficient rate at 175°C; (a) LPP35/BPP30 blends; (b) LPP35/BPP2.5 blends. Dotted lines denote the LVE shear stress growth coefficient η^+ obtained from a Maxwell model fit, using experimental data obtained from linear oscillatory measurements at 175°C.</i> _____	46
Figure 3.8. <i>(a) Flexural moduli and (b) flexural stresses as a function of BPP content for LPP35/BPP2.5 and LPP35/BPP30 blends. Error bars represent 95% confidence intervals.</i> _____	50
Figure 4.1. <i>Typical pressure drop profile during the batch foaming simulations.</i> _____	59
Figure 4.2. <i>SEM images as a function of LPP/BPP/POE wt% composition for: (a) 95/0/5 and (b) 0/95/5 blends prepared in the DSM at 10000x magnification, (c) 70/0/30 and (d) 0/70/30 blends prepared in the DSM at 1000x magnification, and (e) 70/0/30 and (f) 0/70/30 blends prepared in the Haake at 1000x magnification.</i> _____	61
Figure 4.3. <i>Shear viscosity as a function of shearing rate for blends containing various amounts of BPP, and for the virgin POE at 210°C.</i> _____	62

Figure 4.4. Representative fit of the Palierne model for 70/30 wt% LPP/POE blends prepared in the DSM.	63
Figure 4.5. (a) Young's moduli and (b) elongation at break as a function of BPP content; ■ TPOs, ◇ PP blends. Error bars represent 95% confidence intervals. Lines are drawn to guide the eye.	65
Figure 4.6. Flexural modulus as a function of BPP content; ◇ PP blends, ■ TPOs. Lines are drawn to guide the eye. Error bars represent 95% confidence intervals.	66
Figure 4.7. Heat of fusion as a function of BPP content for the TPO blends.	67
Figure 4.8. Images captured during the batch foaming process of blends containing 100 wt% branched PP and (b) 100 wt% branched PP with 30% POE from 0 to 0.16 seconds using nitrogen as the blowing agent, $P_{sat} = 2000\text{psi}$, 180°C , $dP/dt=33\text{MPa/s}$.	69
Figure 4.9. Cell density as a function of time; ◇ 100 wt% branched PP blend, ■ 100 wt% branched PP TPO.	70
Figure 4.10. Cell radius as a function of time for 10 randomly selected bubbles for (a) PP matrix blends and (b) TPO blends.	71
Figure 4.11. Maximum cell density and as a function of BPP content for ▨ PP blends, ■ TPOs.	76
Figure 4.12. Cell growth rate as a function of BPP content for ▨ PP blends, ■ TPOs.	76
Figure 4.13. Maximum cell radius as a function of BPP content for ▨ PP blends, ■ TPOs.	75
Figure 5.1. (a) Complex viscosities, η^* and (b) elastic moduli, G' , as a function of frequency, ω , for a commercial TPO resin (-) as well as for 70/30 PP/POE blends containing 20 wt% BPP and: ● 0 wt% talc, ◇ 5 wt% talc, ■ 10 wt% talc, △ 20 wt% talc.	84
Figure 5.2. (a) Young's moduli and (b) elongation at break as a function of BPP content; ○ 0 wt% talc, 5 wt% talc, ▨ 10 wt% talc, ▨▨▨ 20 wt% talc. Error bars represent 95% confidence intervals.	86





Figure 5.3. (a) Flexural moduli, (b) flexural stresses and (c) flexural strains as a function of BPP content;  0 wt% talc,  5 wt% talc,  10 wt% talc,  20 wt% talc. Error bars represent 95% confidence intervals. _____ 87-88

Figure 5.4. Cooling curve showing T_c for blends containing 20% branched PP both with and without 10 wt% talc. _____ 90

Figure 5.5. SEM images at (a) 1000x magnification and (b) 4000x magnification of 70/30 LPP/elastomer with 10 wt% talc. _____ 90-91

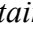
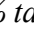
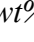
Figure 5.6. Cell densities as a function of time for foamed 70/30 PP/POE blends containing 10 wt % talc and:  0 wt% BPP,  20 wt% BPP,  40 wt% BPP. _____ 92

Figure 5.7. Maximum cell density as a function of BPP content for the TPO blends with 10 wt% talc. _____ 92

Nomenclature

Ca	Capillary number
Ca _{cri}	Critical capillary number
d	Droplet diameter
d _n	Number average diameter of droplets
d _v	Volume average diameter of droplets
ΔE	Activation energy for viscous flow (J/mol)
G'	Elastic or storage modulus (Pa)
G''	Viscous or loss modulus (Pa)
G' _d	Dynamic modulus of the dispersed phase (Pa)
G'' _m	Dynamic modulus of the matrix (Pa)
ΔG _{mix}	Gibbs free energy change of mixing
ΔH _{mix}	Enthalpy change of mixing
k	Viscosity ratio $k = \frac{\eta_d}{\eta_m}$
ΔS _{mix}	Entropy change of mixing
T	Temperature (K)
T _g	Glass transition temperature (K)
t	Time (s)
w _i	Weight fraction of i component in blend

Greek symbols

γ	Shear rate (s^{-1})
η^*	Complex viscosity ($Pa \cdot s$)
η_0	Zero shear viscosity ($Pa \cdot s$)
η_m	Viscosity of the matrix ($Pa \cdot s$)
η_d	Viscosity of the dispersed phase ($Pa \cdot s$)
η_b	Viscosity of the blend ($Pa \cdot s$)
λ	Relaxation time (s)
σ	Interfacial tension (mN/m)
τ	Shear stress (Pa)
ω	Angular frequency (rad/s)
ϕ_i	Volume Fraction of i component phase

Abbreviations

DSC	Differential scanning calorimetry
EPDM	Ethylene-propylene-diene terpolymer
EPR	Ethylene propylene rubber
MFR	Melt flow rate
MFI	Melt flow index
PE	Polyethylene
POE	Polyolefin elastomer
PP	Polypropylene
SBR	Styrene-butadiene rubber

SEM	Scanning electron microscope
TPO	Thermoplastic polyolefin

CHAPTER 1

Introduction

1.1 Polyolefin-Based Polymers in Automotive Applications

The automotive industry in Canada has seen much growth in the past few decades, becoming one of the largest producers of passenger cars in the world. It is estimated that in 2007 the automotive industry in Canada is worth \$36,000 million [1].

A major challenge faced by the industry is to reduce fuel emissions by producing more fuel-efficient vehicles. An effective way to do so is to fabricate automotive components using lightweight materials. Material technology therefore may play a major role in carrying this industry into the future.

Polymers, polymer blends and composites have several noteworthy advantages over traditionally used metals: they offer significant weight savings, as well as good weatherability, processability, and economic benefits. Furthermore, due to the recyclability of polyolefins, the substitution of polyolefin-based polymers in conventional thermosetting applications will allow manufacturers to recycle rejected parts, as well as decrease the environmental burden of disposed vehicles.

Polypropylene (PP) comprises the largest volume of thermoplastic used in automobiles currently on the market [2]. The use of PP in current exterior automotive applications include bumper fascias, body side cladding, and wheel flares. Interior applications of PP can be divided into two categories: hard interiors which contain less than 20% rubber and soft interiors which contain more than 20% rubber. Hard interiors

such as instrument and door trim panels typically consist of PP modified with low levels of an ethylene copolymer. Soft interior PP materials, commonly referred to as thermoplastic polyolefins (TPOs), can be produced either through a reaction process or through physical mixing. TPOs produced by the former process generally have a narrower range of properties and are more expensive than TPOs prepared by the latter. PP foams have just recently gained momentum in the field of automotive applications for use in “under-the-hood” high service temperature parts, as well as interior and cushioning applications.

One major shortcoming of linear PP homopolymers is that they generally do not exhibit the strain hardening behaviour necessary for processes requiring high melt strength, such as foaming, cast and blown film processing, blow molding, and thermoforming. However, this inferior characteristic can be modified by introducing long chain branching [3]. A second shortcoming of PP is its poor low-temperature ductility, which can be improved by the introduction of a rubbery phase in the PP matrix. Of particular interest in generating PP-based materials that have superior properties and processability is the production of blends of linear isotactic PP homopolymer, branched PP homopolymer, and metallocene-based poly(ethylene- α -olefin) copolymers. The following sections outline the basic characteristics of these materials.

1.2 Linear and Branched Polypropylene

Polypropylene, one of the polymer industry’s four major commodity thermoplastics, has become one of the cheapest plastics on the market today. PP homopolymer, a highly crystalline low-density polymer, is commonly used in

applications where high strength and high stiffness are required, such as injection moulded products, fibres, film and pipes [4]. The tacticity of the PP resin is dependent on the production method, including the type of catalyst used. Due to the poor mechanical properties of atactic PP and the difficulties in processing syndiotactic PP, isotactic PP is most commonly used in industrial applications.

Branched polypropylene is commonly synthesized either by high-energy irradiation (electron beam irradiation), the addition of peroxide as an initiator, or a combination of the two processes [5]. Another method that has successfully produced branched PPs is reactive extrusion with a multifunctional monomer and peroxide. A recent comparison between a linear and branched PP with the same molecular weight revealed that the melt strength of the branched PP was approximately ten times higher than that of the linear PP [6] due to the increased entanglements in the presence of branching. This makes branched PP more attractive for applications requiring high melt strength, such as thermoforming, film processing and foaming. In spite of this, the economic cost associated with using branched PPs has deterred their commercial use.

1.3 Polypropylene-based blends

Even though PP offers many advantages, it suffers from brittle failure, especially at low temperatures, making it inadequate for applications where good impact properties are essential. Thermoplastic polyolefins (TPOs), consisting of a PP matrix with a dispersed rubbery phase, display improved properties over their virgin components. The rubber particles that are dispersed in the polyolefin matrix serve to concentrate stresses, and initiate local yielding in the matrix. Polyolefin elastomers (POEs) have been used

extensively in the plastics industry as impact modifiers for brittle polymers such as PP. These polymers are traditionally made with Ziegler-Natta chemistry and include copolymers such as EPDM (ethylene propylene diene monomer) and EPR (Ethylene propylene rubber). Recently, a new class of single-site catalyst based metallocene ethylene- α -olefin copolymers have emerged which offer better control of molecular weight, chain branching and co-monomer content [7]. This breakthrough has enabled the production of tailor-made copolymers with unique properties such as good flexibility, low temperature ductility, low crystalline fraction and thermoplastic and elastomeric behaviour [7,8].

1.4 Foaming of Polyolefins

Polyolefin foams are of interest in various industrial applications due to their superior properties over other commercially available thermoplastics. PP foams specifically show higher strength than polyethylene foams, and better impact strength than polystyrene foams, while providing a higher service temperature range and maintaining good chemical resistance [9]. Due to their superior characteristics, it is expected that foamed PP products will find a number of applications in the food and automobile industry. What is of significant interest in the context of automotive applications, is that these foams have very low density, and can thus be used to produce parts that are extremely light-weight, leading to increased fuel efficiency.

1.5 Objectives and Outline

The motivation of this study was the expressed desire by an automotive parts manufacturer to use thermoplastic olefin foams as part of their bumper fascia assembly, in an effort to reduce the amount of material required, resulting in increased cost-effectiveness and decreased weight of the part. Furthermore, TPOs are also finding increased use in interior components, mainly panels and dashboards, which are usually thermoformed. These applications typically require materials with enhanced melt strength, which can provide improved processability.

In this work high melt strength branched PPs are examined as a means towards improving the processability of TPOs in the aforementioned applications. Given their high cost and their shortcomings in terms of mechanical properties, branched PPs are blended at various proportions with a conventional linear isotactic PP homopolymer of relatively low molecular weight, to provide a suitable matrix for the TPOs.

This thesis consists of six chapters. A literature review on polyolefin blends and foaming technology is shown in Chapter 2. Chapter 3 presents the rheological and physical properties of mixtures of linear and branched PP, which constitute the matrix for the TPO blends analyzed in the rest of the thesis. A detailed investigation into the morphology, properties and foaming behaviour of the TPOs follows in Chapter 4. The effect of talc filler is investigated in Chapter 5.

The thesis ends with Chapter 6 which summarizes the main conclusions of the work and provides recommendations for future work.

1.6 References

1. Automobile Manufacturers in Canada, Datamonitor (2004).
2. Market Search's Automotive Plastics Report (2001).
3. Gotsis, A.D. and B.L.F. Zeevenhoven, *Polym Eng Sci*, 44, 973 (2004).
4. Karger Kocsis, J., *Polypropylene Structure, Blends and Composites, Ver. 2*, London: Chapman & Hall (1995).
5. Gotsis, A.D. and B.L.F. Zeevenhoven, *Polym Eng Sci*, 45, 1512 (2004).
6. De Maio, V.V. and D. Dong, *SPE Antec Tech Pap*, 44, 973 (1997).
7. Jokela, K., Vaananen, A., Torkkeli, M., Starck, P., Serimaa, R., Lofgren, B., and J. Sepala, *J Polym Sci Pol Phys*, 39, 1860-1875 (2001).
8. Perez, E., Benavente, R., Quijada, R., Narvaez, A., and G.B. Balland, *J Polym Sci Pol Phys*, 38, 1440 (2000).
9. Park, C.B. and L.K. Cheung, *Polym Eng Sci*, 37, 1 (1997).

CHAPTER 2

Literature Review

2.1 Polymer Blends

A polymer blend is essentially a mixture of two or more polymers or copolymers, which may be termed either miscible or immiscible. Completely miscible blend systems show unlimited solubility of the components and zero interfacial tension resulting in a homogeneous blend; conversely, immiscible systems show limited solubility and a finite interfacial tension resulting in two phases [1]. At the molecular level, polymer blend systems are generally immiscible; however, if there is enough adhesion between the separate phases, these blends can frequently be labelled mechanically compatible. Incompatible polymers may exhibit a reduction in mechanical properties with respect to the individual components due to a coarser morphology which reduces the mechanical abilities of the blend [1]. Compatible polymers have been known to display improved mechanical properties which are averages of the individual components, and in certain instances, these properties may exceed the properties of the base components through synergistic effects [1].

The shortcomings of using PP in industrial applications are well known. Due to the high glass transition temperature and large spherulite dimensions, isotactic PP displays inadequate impact energy at lower temperatures [2]. The addition of a rubbery phase generally produces blends with improved mechanical properties such as increased elongation and decreased tensile strength at break. High flow rate isotactic

polypropylene is considerably more difficult to impact modify than low melt flow rate polypropylene. However, in terms of industrial applications such as injection foaming, high flow rate materials are desired.

There has been extensive research on isotactic polypropylene and poly(ethylene- α -olefin) copolymer blends, and studies have found that these materials form compatible blend systems [3-5]. Furthermore, superior mechanical properties can be observed under suitable processing conditions where the dispersed rubber particles approach sub-micron sizes [5]. Although the majority of research on thermoplastic polyolefins (TPOs) involved low melt flow rate (high molecular weight) PP with ethylene- α -octene copolymer blends, [6], high melt flow rate PP/ ethylene- α -olefin blends are also important because of their applicability in injection molding applications in the automotive industry [7]. There has been little research done with high melt flow rate PP, although these blends seem to be the most promising for large commercial applications.

2.1.1 Determination of Polymer Miscibility

Thermodynamically, blends are designated miscible if they form a single phase. This classification requires that the second derivative of the Gibbs free energy of mixing must be positive, given by [8].

$$\Delta G_{mix} = \Delta H_{mix} - T\Delta S_{mix} \quad (1)$$

$$\frac{\partial^2 \Delta G_{mix}}{\partial \phi^2} > 0 \quad (2)$$

where ΔG_{mix} is the change of Gibbs free energy of mixing, T is the system temperature, and ΔH_{mix} and ΔS_{mix} are the changes in enthalpy and entropy, respectively.

There are a variety of methods employed in an effort to determine the miscibility of blended systems, including the presence of a single glass transition temperature (T_g). The glass transition temperature represents the temperature at which the energy in the polymeric chains is equal to the forces acting on it. Below this temperature, motion is restricted to vibrational, rotational and short translational movement along the polymer chain. If a polymer blend system exhibits only one T_g , the blends are generally regarded as a miscible system.

To determine the glass transition temperatures, Differential Scanning Calorimetry (DSC) is often used. However, since the glass transition temperature in polyolefins is too low to be reliably detected via DSC, the miscibility of the system can also be assessed by studying its melting and crystallization behaviour [9]. In this case, the occurrence of a shift in the melting transition of the crystalline component in a blend indicates some degree of miscibility.

There are also a variety of rheological methods frequently used in an effort to determine polymer-polymer miscibility, and the majority of these methods involve the manipulation of data obtained from oscillatory rheology. One commonly employed method is the use of the weighted relaxation spectra [10-12]. Blends are generally regarded as miscible if the spectra, plotted as a function of relaxation time, exhibit single peaks. If the blend is immiscible, a second relaxation mechanism, attributed to the deformation of the dispersed phase appears at higher relaxation times. Additionally, Cole-Cole plots, representing loss viscosity versus storage viscosity, have been used as a tool to determine miscibility using the same oscillatory rheology data [13]. Blends that produce Cole-Cole plots with semicircular relationships are considered miscible [13-15].

Blends that adhere to the log-additivity rule, shown in Equation 2, are also considered to be miscible [14].

$$\log \eta_b = \sum_i w_i \log \eta_i \quad (2)$$

where η_b is the blend viscosity, η_i is the viscosity of blend component i , and w_i is the weight fraction of blend component i .

2.2 Morphology of Polymer Blends

The morphology of immiscible polymer blends play a crucial role in influencing the properties of the blend. Unfortunately, the mechanisms of droplet deformation, breakup and coalescence are poorly understood in concentrated viscoelastic systems [1,16]. The type of morphology displayed by polymer blends is largely dependent on the blend composition, the viscoelastic properties of the individual components, and the mixing process. Polymer blends can display droplet matrix morphology, where one phase is dispersed in a continuous phase of the other, or co-continuous morphology [17].

It is widely accepted that morphology affects the toughness of blends [18-20]. There are two modes of failure during impact: crazing, which occurs in polymers that are brittle, and yielding, which occurs in ductile polymers. The addition of rubber for toughening increases the crazing behaviour of brittle polymers through type one failure, and through type two failure, the rubber increases the matrix yielding.

At lower temperatures, the properties of PP diminish and it exhibits a brittle mode of failure; alternatively, at higher temperatures a ductile failure mode is dominant. The temperature at which the brittle-ductile transition takes place is called the brittle-ductile transition temperature [21-22]. Generally, polyolefin elastomers exhibit ductile failure at

service temperatures. Since polypropylene exhibits a much higher glass transition temperature than polyolefin elastomers, a blend of the two components should shift the brittle-ductile transition temperature towards lower temperatures. The addition of the rubbery phase improves the ductility of the stiff PP by increasing the energy absorbed during failure.

2.2.1 Droplet Geometry

The morphology of immiscible polymer blends depends largely on the deformability of the dispersed phase; unfortunately the droplet size and distribution during processing are not widely understood. It is generally accepted that an impact modifier for isotactic PP should have an average particle size of one micron or less [23]. Recent studies have shown that in the case of PP/EPDM (ethylene-propylene-diene terpolymer) rubber blends, the effect of particle size depends largely on the mechanism of deformation [24]. Van der Wal *et al.* [24-25] showed that if crazing is the mechanism of deformation, impact strength increases with increasing particle size; however, if shear yielding is the dominant mechanism, the impact strength decreases with increasing particle size. Another study by Jang *et al.* [26] studied PP blends with EPDM or Styrene-butadiene rubber (SBR), and found that the blends with smaller rubber particles were tougher and more ductile than the blends with larger particles.

2.2.2 Droplet Breakup and Coalescence

The phenomenon of particle breakup and coalescence has been widely examined in a variety of polymer blend systems [27-30], and has been the topic of much research since Taylor in 1932 [31-32]. Taylor's pioneering work includes an expression to determine the maximum droplet size of a Newtonian liquid that will remain stable inside another Newtonian liquid undergoing deformation at a given shear rate.

$$Ca = \frac{\dot{\gamma}\eta_m d}{2\sigma} \quad (3)$$

where Ca is the capillary number, $\dot{\gamma}$ is the shear rate, η_m is the viscosity of the matrix, d is the diameter of the droplet, and σ is the interfacial tension. The critical capillary number, Ca_{cri} , is used to describe the critical condition of breakup. If $Ca < Ca_{cri}$, the droplet will keep its equilibrium shape because the viscous force, which tends to break up the droplet, and the interfacial tension, which tries to keep the droplet spherical, are in an equilibrium with each other. If $Ca > Ca_{cri}$, the viscous forces become dominant and the droplets will deform and break up [33].

Coalescence of the dispersed phase also plays a role in determining the final droplet size. It has been reported that an increase in the weight percentage of the dispersed phase increases the droplet diameter due to the higher probability of collisions between the droplets [34-35]. Since the phenomenon of coalescence is directly proportional to the number of collisions, increasing the shear rate may increase the number of collisions in blends with a high dispersed phase leading to an increase in droplet diameter.

The final equilibrium drop diameter is greatly influenced by the viscosity ratio and coalescence as well as the particle breakup. A study of PP/PS blends revealed that

when the dispersed phase is less than 0.5 %, the values predicted by Taylor's model approaches the final droplet diameter [36]. Roland *et al.* [37] studied immiscible two-component polymer blends and found that in addition to collisions between droplets, Brownian motion attributes to coalescence of the dispersed phase.

Additionally, the elasticity of the matrix and droplet phases can have an impact on the droplet size. In viscoelastic systems, the mechanism of droplet deformation and break up is much different than in Newtonian systems, arising from the combination of shear and extensional flow during mixing. Immiscible polymer blends experience dissipative viscous forces as well as forces which resist deformation in the elastic polymers [36]. Bourry *et al.* [38] studied PS/HDPE blends and determined that under dynamic conditions, the interfacial tension will be lower for blends with a more elastic matrix and less elastic dispersed phase.

2.2.3 *Interfacial tension*

Generally, immiscible polymer blends form a stable interface of finite thickness (typically less than 0.1 μm) between the separate phases [39]. Unlike block copolymers where chemical links between the different blocks inhibit phase separation on a macroscopic scale [40], polymer blends form interfaces arising from both inter-diffusion of the macromolecular segments and interfacial chemical bonding if functional groups are present [39].

Low interfacial tension between the phases signifies the tendency of one polymer to wet the other, thereby promoting the interdiffusion of polymer chains. Studies on

PS/PE blends have shown that the interfacial tension values range from 4 to 7 mN/m depending on the molecular weight of both phases [39, 41-43].

There are a variety of techniques used to determine the interfacial tension of polymer blends including the spinning drop, pendant drop and breaking thread techniques [39, 44]. Carriere *et al.* recently used the imbedded fiber retraction method to determine the interfacial tension of polypropylene/polyolefin blends [45] and found that the values of interfacial tension ranged from 0.56 to 1.07 mN/m. The interfacial tension values decreased with increasing co-monomer content in the polyolefin elastomer (POE), resulting in more miscible blends. This result is in agreement with previous findings [46-48]. In addition to experimentally determining interfacial tension values, a model such as the Palierne emulsion model has been widely used [49,50].

2.3 Relating Morphology to Rheology: The Palierne Emulsion Model

The rheology of multiphase polymer systems is very complex due to numerous factors including the component properties, interfacial tension, morphology, as well as the strain history during processing. In an effort to predict the morphology of non-dilute suspensions of viscoelastic droplets in a viscoelastic matrix, there have been a number of proposed linear viscoelastic rheological emulsion models. Oldroyd's emulsion model, first proposed in 1953 [51], showed that the elasticity of emulsions are due to interfacial tension effects, assuming all suspensions are dilute, the droplets can only slightly deform, and there are negligible inertia and hydrodynamic interactions.

An extension of the Oldroyd emulsion model was proposed by Palierne [49, 50] which takes into account dipole-type particle interactions as well as effects of particle

size distribution. This model describes the complex modulus, $G^*(\omega)$, of incompressible viscoelastic emulsions as a function of the complex moduli of both phases, the ratio of interfacial tension, the droplet size, and the droplet size distribution:

$$G^*(\omega) = G_m^*(\omega) \frac{1 + 3 \sum_i \phi_i H_i^*(\omega)}{1 - 2 \sum_i \phi_i H_i^*(\omega)} \quad (4)$$

where $H_i^*(\omega)$ is given by

$$H_i^*(\omega) = \frac{8 \left(\frac{\alpha}{d_i} \right) \left[2G_m^*(\omega) + 5G_d^*(\omega) \right] + \left[G_d^*(\omega) - G_m^*(\omega) \right] \left[16G_m^*(\omega) + 19G_d^*(\omega) \right]}{80 \left(\frac{\alpha}{d_i} \right) \left[G_m^*(\omega) + G_d^*(\omega) \right] + \left[2G_d^*(\omega) + 3G_m^*(\omega) \right] \left[16G_m^*(\omega) + 19G_d^*(\omega) \right]}$$

where $G_m^*(\omega)$ and $G_d^*(\omega)$ are the complex moduli for the matrix and the dispersed phase, respectively, α is the interfacial tension, and ϕ_i is the volume fraction of droplets with diameter d_i .

The Palierne emulsion model also takes into account parameters related to the deformability of the interface. The main assumption of this model is that the droplet deformation remains small; therefore, the theory only predicts linear viscoelastic behaviour, and can only be used with experimental data obtained in the linear range (i.e., obtained from oscillatory measurements using small strain amplitudes).

In the event of constant interfacial tension and uniform particle size, it is possible to obtain a simplified expression for the complex shear modulus of the emulsion.

$$G^*(\omega) = G_m^*(\omega) \frac{1 + 3\phi H(\omega)}{1 - 2\phi H(\omega)} \quad (5)$$

Bousmina and Muller [52] showed that the volume average diameter, d_v , takes into account most of the particle size distribution effects, more so than the number average diameter d_n . Using this assumption, a further simplification of the model expresses the complex modulus of the blend as a function of the moduli of both components [53].

$$G^* = G' + iG'' \quad (6a)$$

$$G' = \frac{1}{B_1^2 + B_3^2} [G'_m (B_1 B_2 + B_3 B_4) - G''_m (B_1 B_4 - B_2 B_3)] \quad (6b)$$

$$G'' = \frac{1}{B_1^2 + B_3^2} [G'_m (B_1 B_4 - B_2 B_3) + G''_m (B_1 B_2 + B_3 B_4)] \quad (6c)$$

where the constants B_i and C_i are given by,

$$B_1 = C_1 - 2\phi C_3$$

$$B_2 = C_1 + 3\phi C_3$$

$$B_3 = C_2 - 2\phi C_4$$

$$B_4 = C_2 + 3\phi C_4$$

$$C_1 = 80 \left(\frac{\alpha}{d_v} \right) (G'_m + G'_d) + 48(G_m'^2 + G_m''^2) + 38(G_d'^2 + G_d''^2) + 89(G'_m G'_d - G''_m G''_d)$$

$$C_2 = 80 \left(\frac{\alpha}{d_v} \right) (G''_m + G''_d) + 96G'_m G''_m + 76G'_d G''_d + 89(G''_m G'_d + G'_m G''_d)$$

$$C_3 = 8 \left(\frac{\alpha}{d_v} \right) (2G'_m + 5G'_d) - 16(G_m'^2 + G_m''^2) + 19(G_d'^2 + G_d''^2) - 3(G'_m G'_d - G''_m G''_d)$$

$$C_4 = 8 \left(\frac{\alpha}{d_v} \right) (2G''_m + 5G''_d) - 32G'_m G''_m + 38G'_d G''_d - 3(G''_m G'_d + G'_m G''_d)$$

This simpler model contains no empirical parameters, and allows the prediction of linear viscoelastic properties of immiscible polymer blends entirely from

experimentally established data by using the complex modulus of both phases, the particle size, the volume fraction of droplets, and the interfacial tension.

Numerous researchers have used the Palierne model with various blends systems, and have obtained good agreement between experimental data and the model predictions. Bousmina *et al.* [53] studied a PS/PE 70/30 wt% blend and found that the value for interfacial tension, 5.2 ± 0.2 mN/m, was the typical value reported in literature for this blend [39]. They also examined the properties of the inversed blend, PS/PE 30/70 wt%, where the matrix is less viscous than the dispersed phase. In this case, the emulsion model could not be used to verify the interfacial tension value because the secondary plateau did not appear, and the droplets could not be deformed.

Kontopoulou *et al.* [7] used the Palierne emulsion model to fit viscoelastic curves of the blends to estimate the interfacial tension of ethylene- α -olefin copolymer/polypropylene blends. The values of interfacial tension were found to be 0.64 and 0.6 mN/m for PP blends with butene and octene copolymers, respectively. These results are in good agreement with previously reported values determined using mechanical methods [45].

2.4 Foaming Theory

In order to characterize plastic foams, researchers have devised a classification system based on cell sizes/cell densities, and bulk foam densities. Foams with large cell sizes of 300 μm and up, with cell densities the order of 10^6 cells/cm³ are classified as conventional foams, while small celled foams displaying cell sizes of 10 μm and cell densities of 10^9 cells/cm³ are classified as microcellular foams. The third category, fine-

celled foams, accounts for foams with cell sizes and densities which fall between the conventional and microcellular foams.

Bulk foam densities are also used as a classification system, and are divided into four categories. The foams with an expansion of less than 4 fold are considered high density foams; medium density foams fall between 4 fold and 10 fold; low density foams between 10 fold and 40 fold, and foams with more than 40 fold expansions are labelled very low density foams. High-density foams are typically used for structural purposes such as wires and cables, while low-density foams are primarily used in cushion packaging. [54]

2.4.1 Foaming Mechanism – Nucleation, cell growth and coalescence

Foaming generally occurs in three major steps: nucleation, bubble growth, and stabilization. Nucleation involves the formation of expandable bubbles in a polymer melt super-saturated with a blowing agent. If a physical blowing agent, such as nitrogen is used, the agent is dissolved into the polymer at higher pressures. Alternatively, if a chemical blowing agent, such as azodicarbonamide is used, this agent releases gas at a specific decomposition temperature and the gas is then dissolved in the polymer. After nucleation, the bubble will continue to grow as the blowing agent diffuses into it until it stabilizes or ruptures [54]. Cell growth is completed when there is no longer any diffusion occurring, and there is force equilibrium between the pressure in the cell, the surrounding pressure, and the surface tension of the polymer, or when the polymer becomes frozen.

There are two major types of nucleation in polymer foaming: homogeneous and heterogeneous. Heterogeneous nucleation takes place at the phase boundaries between immiscible blends, which have a lower free energy barrier for nucleation; whereas homogeneous nucleation refers to classical nucleation theory used to describe the nucleation behavior in single component or miscible blended systems. However, heterogeneous nucleation may also occur due to impurities in the sample itself, or due to the type of nucleating agent used, such as talc, sodium benzoate or carbon dioxide.

2.4.2 Cell Growth and Coalescence

Numerous studies have been done to investigate the factors that govern cell growth and coalescence. Otsuki and Kanai [55] modeled foaming behaviour using a PP system with carbon dioxide foaming agent, and found that the linear viscoelastic characteristics of the polymer melt influence the bubble growth rate; however, there are a number of other factors which have a larger effect on this rate such as the bubble nucleus population density, surrounding pressure, initial dissolved foaming agent concentration, and the diffusion coefficient. Using a polystyrene/carbon dioxide system, Leung *et al.* [56] modeled foaming behaviour and found that higher diffusivity of the blowing agent leads to an increase in the cell growth rate; however at longer times, the cells grew large enough that further growth of the bubbles was limited by low gas contents within the shells. Both studies found that neither the strain hardening characteristics of the polymer melt, nor the surface tension, had a significant effect on the rate of volume expansion [55, 56]. However, Taki *et al.* [57] analyzed four patterns of bubble coalescence in polymer

foaming processes, and found that the coalescence time was longer when the strain hardening behaviour was more pronounced.

2.4.3 Foam processing

The main goal in producing polymer foams is to construct lightweight materials without sacrificing any mechanical or physical properties. This can be done through a variety of processes including the less widely used leaching and sintering processes; however, the majority of commercial polyolefin foams are produced by the expansion process [54]. This process relies on the expansion of a gaseous phase dispersed in the polymer melt, where the gaseous phase may be generated by the separation of a dissolved gas, the vaporization of a volatile liquid, or the release of a gas from a chemical reaction. In addition to extrusion foaming, polymer foams can be produced by compression moulding, injection moulding and the less widely used rotomoulding.

The main issues with foamed plastics involve their inherent low structural strength and rigidity due to the void space present in the foamed structure. It is known that the presence of smaller cells and higher uniformity in cellular structure gives better mechanical and thermal properties [58, 59]. Therefore, much research has been focused recently on achieving a high cell population density. It has been found that the decrease of cell size to 10 μm can greatly increase the toughness, impact strength and fatigue life of foamed plastics [60, 61]. In an effort to obtain these fine-cell foamed structures, it is crucial to increase the number of nucleated cells in the polymer melt. The addition of a foaming agent aides to increase the number of nucleation sites available in the melt,

which in turn can enhance cell nucleation due to lower activation energy at these locations [62, 63].

These very fine celled foams can be produced using the microcellular foaming process. This process, outlined in Figure 2.1 involves the introduction of the blowing agent (gas) into the polymer melt at elevated temperatures and pressures, as well as the mixing, diffusion, nucleation and subsequent cell growth of the mixture as a result of thermodynamic instability in the system [64].

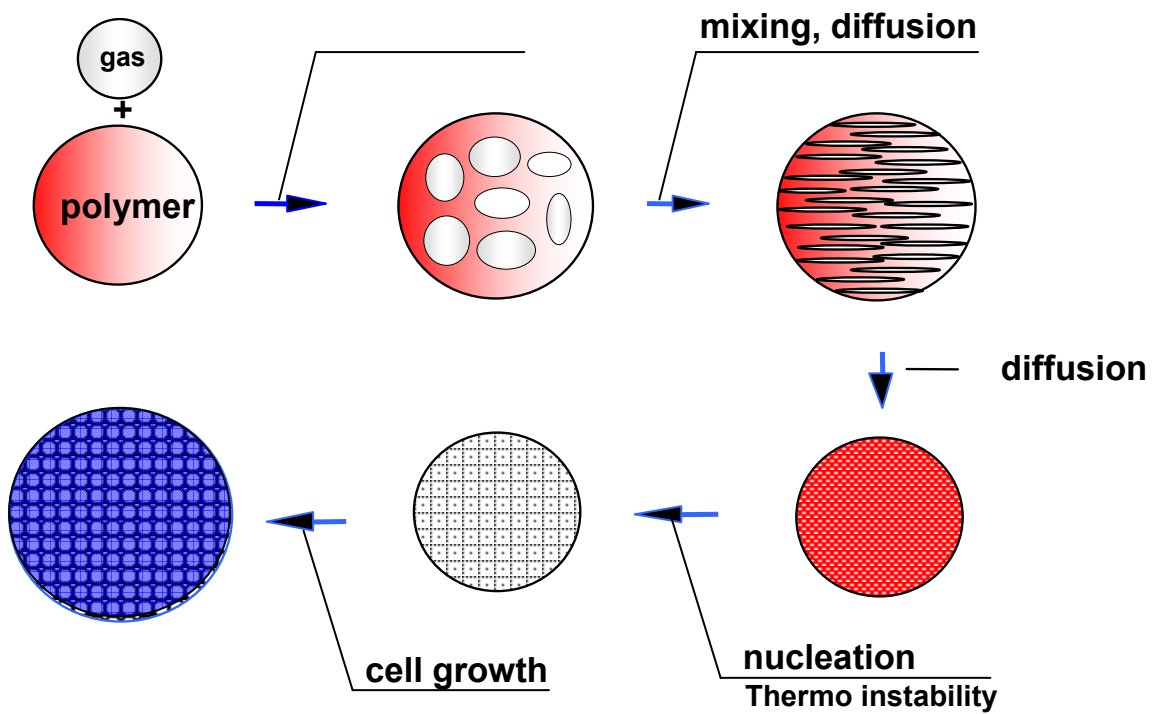


Figure 2.1. Diagram of the microcellular foaming process [64].

2.4.4 Polyolefin foams

For many years, polyethylene (PE) has been the polyolefin of choice for commercial thermoplastic foam production. PE exhibits excellent mechanical properties,

as well as good temperature stability and high chemical resistance. The major advantage of using PE over PP is that conventional linear PP resins possess a narrow processing window due to their inherent low melt strength. During foaming, this shortcoming causes the cell walls separating the foamed bubbles to become weak and therefore susceptible to coalescence and rupture. To further improve the thermoformability and foamability of the resins, much research has concentrated on material modification on existing resins or new PP resins altogether in an effort to broaden this window.

One traditional way to increase melt strength is to induce crosslinking [65]. By means of crosslinking PP resins, researchers were able to significantly improve the volume expandability, cell uniformity and thermoformability of the foams [65]. Nojiri *et al.* [66] crosslinked PP with triacrylate or trimethacrylate, and produced a foam with good thermoformability, high elongation, a uniform fine cell structure, and a low density of 0.035 g/cm^3 . However, much research has been directed away from this method due to the non-recyclability of the final product due to crosslinking.

In addition, long chain branching has demonstrated ability to improve the melt strength of the PP material, and these high melt strength PP resins have also displayed improved foamability and thermoformability [67-69]. Park *et al.* [69] used a PP blend with two components in their study: the major component was a slightly branched PP, and the minor component was highly branched PP with a higher molecular weight. Using a sheet foam processing method, an acceptable foamed sheet was produced with densities of $0.04 - 0.4 \text{ g/cm}^3$. This method of incorporating small amounts of high melt strength PP into a predominately linear PP melt may prove to be the most successful method in producing suitable PP foams for commercial applications.

Recently, there has been significant progress in the foaming of immiscible polyolefin blends, particularly PE/PP blends. Rachtanapun *et al.* [70,71] showed that using CO₂ in a batch process HDPE/PP blends were easier to foam than neat polymers, and attributed this observation to possible heterogenous nucleation at the interface between the two immiscible blends. Using azodicarbonamide as a blowing agent, Tejada *et al.* [72] also studied the foaming of HDPE/PP blends and found that the minimum cell size of the corresponding foams was obtained at the 50/50 composition. This result was attributed to the dispersed polymer phase acting as a nucleating site to produce foams with smaller cell sizes. In spite of the many recent investigations, the issue of foaming of polymer blends is still a largely untackled one, with many conflicting observations and reports. The complex nature of the morphology and the rheological characteristics of the blends further impedes the correct interpretation of the results. A rigorous approach, where all factors involved in the nucleation, cell growth and coalescence processes are considered systematically, is needed.

2.5 References

1. L.A. Utracki, *Two-Phase Polymer Systems*, New York: Hanser (1991).
2. J. Karger Kocsis, *Polypropylene: Structure, Blends and Composites, Ver.1*, London: Chapman & Hall (1995).
3. C.J. Carriere and H. C. Silvis, *J Appl Polym Sci*, 66, 1175 (1997).
4. A.L.N. Da Silva, M.C.G.. Rocha, F.M.B. Coutinho, R. Bretas and C. Suracchio, *J Appl Polym Sci*, 75, 692 (2000).
5. T.C. Yu, *Polym Eng Sci*, 41, 656 (2001).
6. N. Kukaleva, M. Jollands, F. Cser and E. Kosior, *J Appl Polym Sci*, 76, 1011 (2000).
7. M. Kontopoulou, W. Wang, T.G. Gopakumar and C. Cheung, *Polymer*, 44, 7495 (2003).
8. D.R. Paul and S. Newman (Eds), *Polymer Blends, Ver.2*, New York: Academic Press Inc. (1978).
9. A.L.N. Da Silva, M.I.B. Tavares, D.P. Politano, F.M.B. Coutinho and M.C.G. Rocha, *J Appl Polym Sci*, 66, 2005 (1997).
10. J.D. Ferry, *Viscoelastic Properties of Polymers, 3rd ed.*, New York: Wiley (1980).
11. Y. Fang, P.J. Carreau and P.G. Lafleur, *Polym Eng Sci*, 45 1254 (2005).
12. C. Lacroix, M. Aressy and P.J. Carreau, *Rheol Acta*, 36 416 (1997).
13. K.S. Cole and R.H. Cole, *J Chem Phys*, 9 341 (1941).
14. L.A. Utracki and B. Schlund, *Polym Eng Sci*, 27, 1512 (1987).
15. H. Kwag, D. Rana, K. Cho, J. Rhee, T. Woo, B.H. Lee and S. Choe, *Polym Eng Sci*, 40, 1672 (2000).
16. L.A. Utracki, *Polymer Alloys and Blends*, New York: Hanser (1989).
17. D.R. Paul and J.W. Barlow, *J Macromol Sci, Rev Macromol Chem*, C18, 109 (1980).
18. C.B. Bucknall, *Toughened Plastics*, London:Appl.Sci.Publ. (1977).

19. S.Wu, *J Polym Sci*, 21, 699 (1983).
20. S.Wu, *Polymer*, 26, 1855 (1985).
21. S.Wu and A. Margonlina, *Polymer*, 31, 972 (1990).
22. A. van der Wal, J.J. Mulder, J. Oderkerk and R.J. Gaymans, *Polymer*, 39, 6781 (1998).
23. T.C. Yu, *Polym Eng Sci*, 41, 656 (2001).
24. A. van der Wal, and R.J. Gaymans, *Polymer*, 40, 6067 (1999).
25. A. van der Wal, A.J.J. Verheul and R.J. Gaymans, *Polymer*, 40, 6057 (1999).
26. B.Z. Jang, D.R. Uhlmann and J.B.V. Sande, *Polym Eng Sci*, 25, 643 (1985).
27. H.J. Karam and J.C. Bellinger, *Ind Eng Chem Fund*, 7, 576 (1968).
28. R.W. Flumerflet, *Ind Eng Chem Fund*, 11, 312 (1972).
29. J.J. Elmendorp and A.K. Van Der Vegt, *Polym Eng Sci*, 26, 1332 (1986).
30. B.D. Favis, *J Appl Polym Sci*, 39, 285 (1990).
31. G.I. Taylor, *Proc R Soc A*, 138, 41 (1932).
32. G.I. Taylor, *Proc R Soc A*, 146, 501 (1934).
33. P. Martin, P.J. Carreau and B.D. Favis, *J Rheol*, 44, 569 (2000).
34. B.D. Favis and D. Therrien, *Polymer*, 32, 1474 (1991).
35. N. Kukaleva, M. Jollands, F. Cser and E. Kosior, *J Appl Polym Sci*, 76, 1011 (2000).
36. J.J. Elemendorp and A.K. Van Der Vegt, *Polym Eng Sci*, 26, 1332 (1986).
37. C.M. Roland and G.G.A. Bohm, *J Polym Sci:Polym Phys*, 22, 79 (1984).
38. D. Bourry and B.D. Favis, *J Polym Sci:Polym Phys*, 36, 1889 (1998).
39. S. Wu, Marcel Dekker, Inc. (1982).

40. C. Neumann, D. R. Loveday, V. Abetz and R. Stadler, *Macromolecules*, 31, 2493 (1998).
41. C.C. Chen and J.L. White, *Polym Eng Sci*, 33, 923 (1993).
42. N. Mekhilef, B.D. Favis and P.J. Carreau, *J Polym Sci:Polym Phys*, 35, 293 (1997).
43. N. Mekhilef, P.J. Carreau, B.D. Favis, P. Martin and A. Ouhal, *J Polym Sci:Polym Phys*, 38, 1359 (2000).
44. H. Liang, R. Xu, B.D. Favis and P. Schreiber, *J Polym Sci; Polym Phys*, 38, 2096 (2000).
45. C.J. Carriere and H. C. Silvis, *J Appl Polym Sci*, 66, 1175 (1997).
46. M. Yamaguchi, H. Miyata and K.H. Nitta, *J Appl Polym Sci*, 62, 87 (1996).
47. M. Yamaguchi, H. Miyata and K.H. Nitta, *J Polym Sci; Polym Phys*, 35, 953 (1997).
48. M. Yamaguchi, H. Miyata, K.H. Nitta and T. Masuda, *J Appl Polym Sci*, 63, 467 (1997).
49. J.F. Palierne, *Rheol Acta*, 29, 204 (1990).
50. J.F. Palierne, *Rheol Acta*, 30, 497 (1991).
51. J.G. Oldroyd, *Proc Roy Soc London*, A218, 122 (1953).
52. M. Bousmina and R. Muller, *J Rheol*, 37, 663 (1993).
53. M. Bousmina, P.B. Bataille, S. Sapiaha and H.P. Shreiber, *J Rheol*, 39, 499 (1995).
54. C.P. Park, *Handbook of Polymeric Foams and Foam Technology*, Chap. 9, 187-242, D. Klempner and K.C. Frisch, eds., New York: Hanser (1991).
55. Y. Otsuki and T. Kanai, *Polym Eng Sci*, 45, 1277 (2005)
56. S.N. Leung, C.B. Park, D. Xu, H. Li, and R.G. Fenton, *Ind Eng Chem Res*, 45, 7823 (2006).
57. K. Taki, T. Nakayama, T. Yatsuzuka and M. Ohshima, *J Cell Plast*, 39, 155 (2003).

58. D. I. Collias and D. G. Baird, *Polym Eng Sci*, 35, 1167 (1995).
59. D. I. Collias and D. G. Baird, *Polym Eng Sci*, 35, 1178 (1995).
60. F.A. Shutov, *Handbook of Polymeric Foams and Foam Technology*, Chap. 3, 17-46, D. Klemmner and K.C. Frisch, eds., New York: Hanser (1991).
61. D.I. Collias, D.G. Baird and R.J.M. Borggreve, *Polymer*, 25, 3978 (1994).
62. J.S. Colton and N.P. Suh, *Polym Eng Sci*, 27, 485 (1987).
63. J.S. Colton and N.P. Suh, *Polym Eng Sci*, 27, 493 (1987).
64. C.B. Park, *Science and Technology of Microcellular Foaming*, presented at Queen's University, March 2004.
65. Y.D. Lee and L.F. Wang, *J Appl Polym Sci*, 32, 4639 (1986).
66. A. Nojiri, T. Sawasaki and T. Koreeda, U.S. Patent 4 424 296 (1984).
67. C.B. Park, and L.K. Cheung, *Polym Eng Sci*, 37, 1 (1997).
68. J.J. Park, L. Katz and N.G. Gaylord, U.S. Patent 5 149 579 (1991).
69. J.J. Park, L. Katz and N.G. Gaylord, U.S. Patent 5 116 881 (1992).
70. P. Rachtanapun, S.E.M. Selke and L.M. Matuana, *Polym Eng Sci*, 44, 1551 (2004).
71. P. Rachtanapun, S.E.M. Selke, and L.M. Matuana, *J Appl Polym Sci*, 93, 364 (2004).
72. E.H. Tejeda, C.Z. Sahagún, R. González-Núñez and D. Rodrigue, *J Cell Plast*, 41, 417 (2005).

CHAPTER 3

The Rheological and Physical Properties of Linear and Branched Polypropylene Blends^{*}

3.1 Introduction

Polypropylene (PP) is widely used in many processing applications, including extrusion and injection molding. However, PP melts generally do not exhibit the strain hardening behaviour necessary for processes that require high melt strength, such as foaming, cast and blown film processing, blow molding, and thermoforming.

With the development and commercial availability of high melt strength long chain branched PPs new applications have become possible in foaming [1-3], as well as thermoforming [4]. Nevertheless, the cost of branched PPs has deterred their widespread use in industrial operations. The creation of blends of linear and branched PP has the potential to yield new and enhanced materials at a fraction of the cost.

The performance of these blends in foam processing, and in extrusion foaming in particular, is of significant interest. Various studies have indicated that increasing the branched PP content in linear/branched PP blends improves the foaming behaviour of conventional PP and results in a higher cell density [5,6]. Conversely, high-branched PP loadings have resulted in substandard foamability [1]. The addition of branches may also compromise certain mechanical properties, such as strain at break [4]. Therefore, to obtain favourable foaming conditions while maintaining satisfactory mechanical

^{*} A version of the chapter has been published. T.J. McCallum, M. Kontopoulou, C.B. Park, E.B. Muliawan and S.G. Hatzikiriakos, *Polym Eng Sci*, 47, 1133 (2007).

properties, an optimal content of branched PP must be determined. Recent efforts have shown that a peak in cell concentration occurs when 25 wt% branched PP is added to linear PP [7].

It is well known that the presence of branching generally affects the physical properties of polyolefins. As extensive investigations have shown, the phase behaviour of polyethylene blends depends heavily on the presence of short or long chain branching [8-15]. Elongational properties have been documented primarily for linear low-density polyethylene (LLDPE) and low-density polyethylene (LDPE) blends. Research has shown that the addition of LDPE to LLDPE generally enhances the melt strength as a result of the long chain branching character of LDPE [9-11]. This increase in melt strength has been attributed to the immiscibility of the blend components [16,17]. Increases in the melt strength of high-density polyethylene (HDPE)/LDPE blends have also been reported [9]. It has been suggested that the addition of metallocene catalyzed HDPE, which has small amounts of long chain branching, to metallocene catalyzed LLDPE may provide better performance in blow molding, vacuum forming, and perhaps even film production [12].

In spite of the abundance of recent studies on linear and branched PP blends, detailed investigations of their rheological and physical properties have been relatively scarce; those that have been undertaken have concentrated almost exclusively on the blends' rheology in extension. It has been commonly reported that the extensional rheology of these mixtures is highly sensitive to the presence of long chain branches [4,7,18]. Strain hardening behaviour was observed, even at contents of branched PP as

low as 10% [18]. Most of this work has examined blend formulations that are suitable for extrusion foaming.

This chapter aims to characterize in detail the rheological properties, phase behaviour, and physical properties of linear and branched polypropylene blends. Our work focuses on blends containing a high melt flow rate (MFR) linear PP as part of an effort to develop a useful material that is suitable for injection foam molding applications.

3.2 Experimental

3.2.1 Materials

One linear and two branched PP samples supplied by Basell (Elkton, MD) were used in this study; Pro-fax PD702 (LPP35) is an injection molding grade linear PP homopolymer. Pro-fax PF814 (BPP2.5) and PF611 (BPP30) are both high melt strength, branched homopolymer PP resins. The former is a foaming grade resin, while the latter is suitable for extrusion coating applications. All PPs used in this work have a density of 902 kg/m^3 . The molecular weight and molecular weight distribution were measured using a Viscotek model 350 high temperature GPC, equipped with a dual angle LS (7° and 90°) viscometer and RI detectors. The properties of all polymers are summarized in Table 3.1.

A series of samples containing a range of branched PP compositions (LPP/BPP 20/80, 40/60, 60/40, and 80/20 by weight) were prepared, as outlined in the blend preparation section. All three pure PP samples were subjected to the same processing history in order to serve as control samples.

Table 3.1. Material Properties.

Material	Trade Name	MFR (g/10 min, 230°C)	M_n (kg/mol)	M_w/M_n
LPP35 (linear PP)	“Pro-fax” PD702	35	36.7	8.4
BPP2.5 (branched PP)	“Pro-fax” PF814	2.5	190	6.2
BPP30 (branched PP)	“Pro-fax” PF611	30	77.5	6.6

3.2.2 Blend Preparation

All blend components were dry-blended with 0.2% antioxidant (Irganox B225 from CibaGeigy). The dry blended formulations were then compounded at 210°C using a Haake PolyLab Rheocord torque rheometer equipped with a Rheomix 610p mixing chamber and roller rotors until the torque profile exhibited steady state behaviour (approximately 6-7 minutes). The Haake was operated at approximately 70% capacity, under a nitrogen blanket to limit PP degradation.

3.2.3 Rheological Characterization

A Carver hydraulic press, heated at 200°C, was used to form compression molded discs that were approximately 2 mm in thickness and 25 mm in diameter. The samples were then characterized with a controlled stress rheometer (ViscoTech by Rheologica) in the oscillatory mode, using parallel plate fixtures 20 mm in diameter at a gap of 1.5 mm. All measurements were carried out under a nitrogen atmosphere to limit degradation and

the absorption of moisture. Time sweeps confirmed that the samples were sufficiently stabilized and did not degrade during the duration of a typical experiment.

Strain sweeps were performed to ensure the measurements were within the linear viscoelastic (LVE) regime. The elastic modulus (G'), viscous modulus (G''), and complex viscosity (η^*) were measured as a function of the angular frequency (ω) at frequencies ranging from 0.04 rad/s – 188.5 rad/s. The rheological characterization of blends consisting of LPP35/BPP2.5 was done at 210°C, in an effort to obtain data approaching the region of terminal flow, whereas the blends consisting of the low-viscosity components with LPP35 and BPP30 were measured at 180°C, in order to improve the accuracy of the measurement at low frequencies, given the low viscosity of the components. To further verify the accuracy of our low-frequency measurements and to determine the zero shear viscosity, creep experiments were performed at stresses between 2-5 MPa, using the same controlled stress rheometer.

To characterize the blends at higher shear rates (20-2000s⁻¹), a twin bore capillary rheometer RH2000 (Bohlin Instruments) was used at 210°C. The shear viscosities were calculated by applying the Bagley and Rabinowitch corrections [19].

Finally, the blends were rheologically characterized in simple extension using an Sentmanat Extension Rheometer (SER) Universal Testing Platform [20,21] from Xpansion Instruments. As described by Sentmanat [22] the SER unit is a dual windup extensional rheometer that has been specifically designed for use as a detachable fixture on a variety of commercially available rotational rheometer host platforms. The particular SER model used in this study was designed for use on a VOR Bohlin rotational rheometer host system.

Specimens were prepared by compression molding the polymer samples between polyester films to a gage of about 1 mm, using a hydraulic press. Individual polymer specimens were then cut to a width of 6.4-12.7 mm. Typical SER extensional melt rheology specimens range from 40-150 mg in mass.

Measurements were conducted at 175°C, slightly above the melting point of the polymers, to ensure that the viscosities of the samples were high enough to prevent sagging. Linear viscoelastic oscillatory measurements were also obtained at 175°C using the VOR Bohlin rotational rheometer, in order to calculate the LVE shear stress growth plot.

3.2.4 Thermal Properties

A TA Instrument Differential Scanning Calorimeter (DSC) Q100 was employed to characterize the thermal properties of the blends. Approximately 5-8 mg of the samples were weighed and sealed in an aluminum hermetic pan, and subsequently heated from 30°C to 200°C at a rate of 5°C/min. They were then held isothermally for 10 minutes to destroy any residual nuclei before cooling at 5°C/min. The melting temperatures and heats of fusion were obtained from a second heating sequence, performed at 5°C/min.

3.2.5 Mechanical Properties

An Instron 3369 universal testing machine was used to determine the tensile properties of all the materials. Measurements were carried out according to the ASTM D638 standard, using type V specimens stamped out from compression molded sheets

prepared at 210°C. Five replicate runs at a crosshead speed of 10 mm/min were completed at each composition to ensure the reproducibility of the results.

Flexural tests were also performed using the Instron 3369, in accordance with ASTM D790, procedure B, at a strain rate of 0.10 (mm/mm)/min. The samples having dimensions 127x12.7x3.2mm were compression molded at 210°C with the hydraulic press. The flexural modulus as well as flexural stresses and strains were calculated from the resulting curves.

3.3 Results and Discussion

3.3.1 Oscillatory Shear Rheology

Figures 3.1 and 3.2 summarize the complex viscosities (η^*) and elastic moduli (G') of the LPP35/BPP30 and LPP35/BPP2.5 blends respectively, as a function of frequency (ω). In both sets of blends, increasing the branched PP content results in higher complex viscosities and higher values of the elastic moduli at the low frequency range.

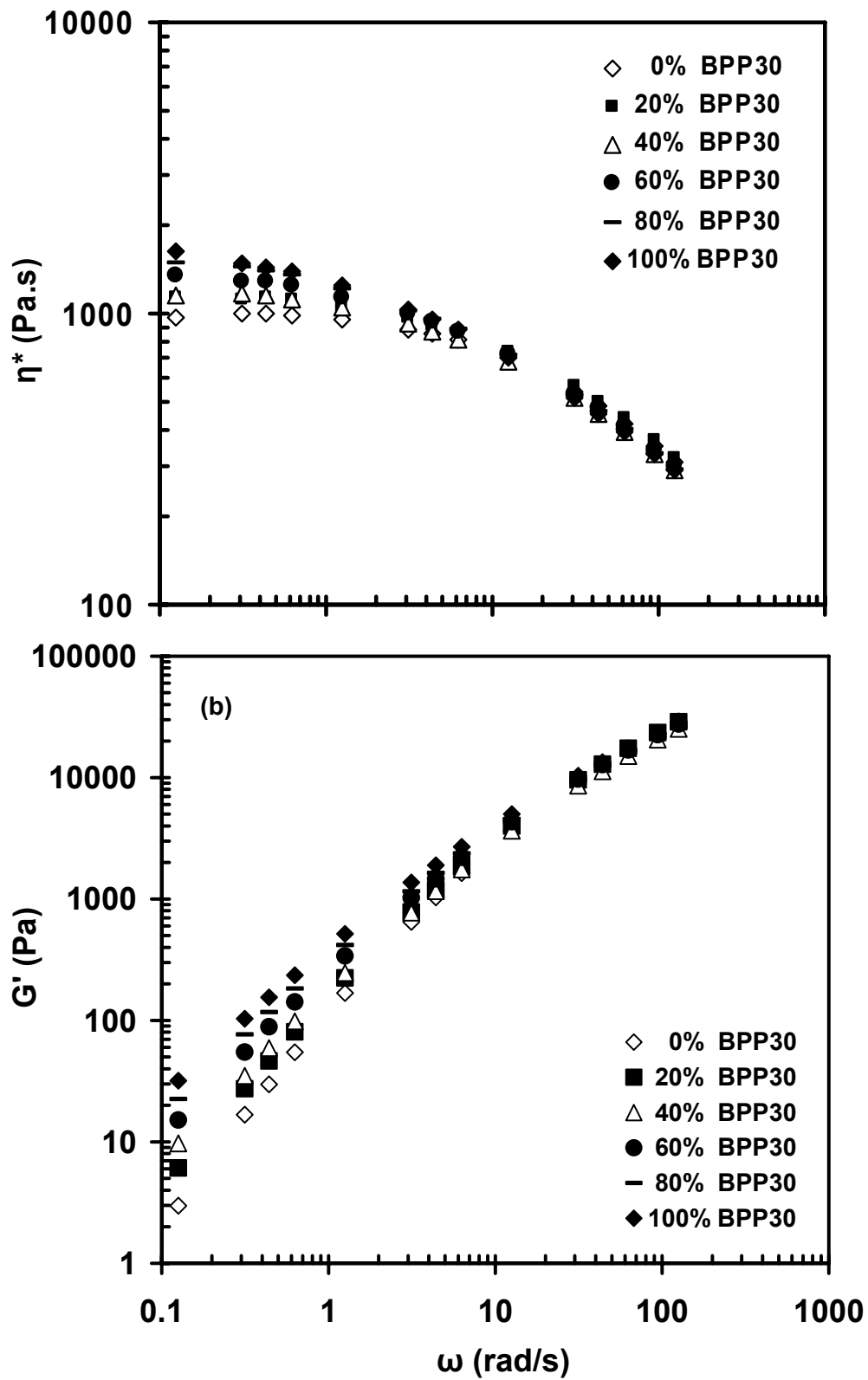


Figure 3.1. (a) Complex viscosities, η^* and (b) elastic moduli, G' , as a function of frequency, ω , for LPP35/BPP30 blends at 180°C.

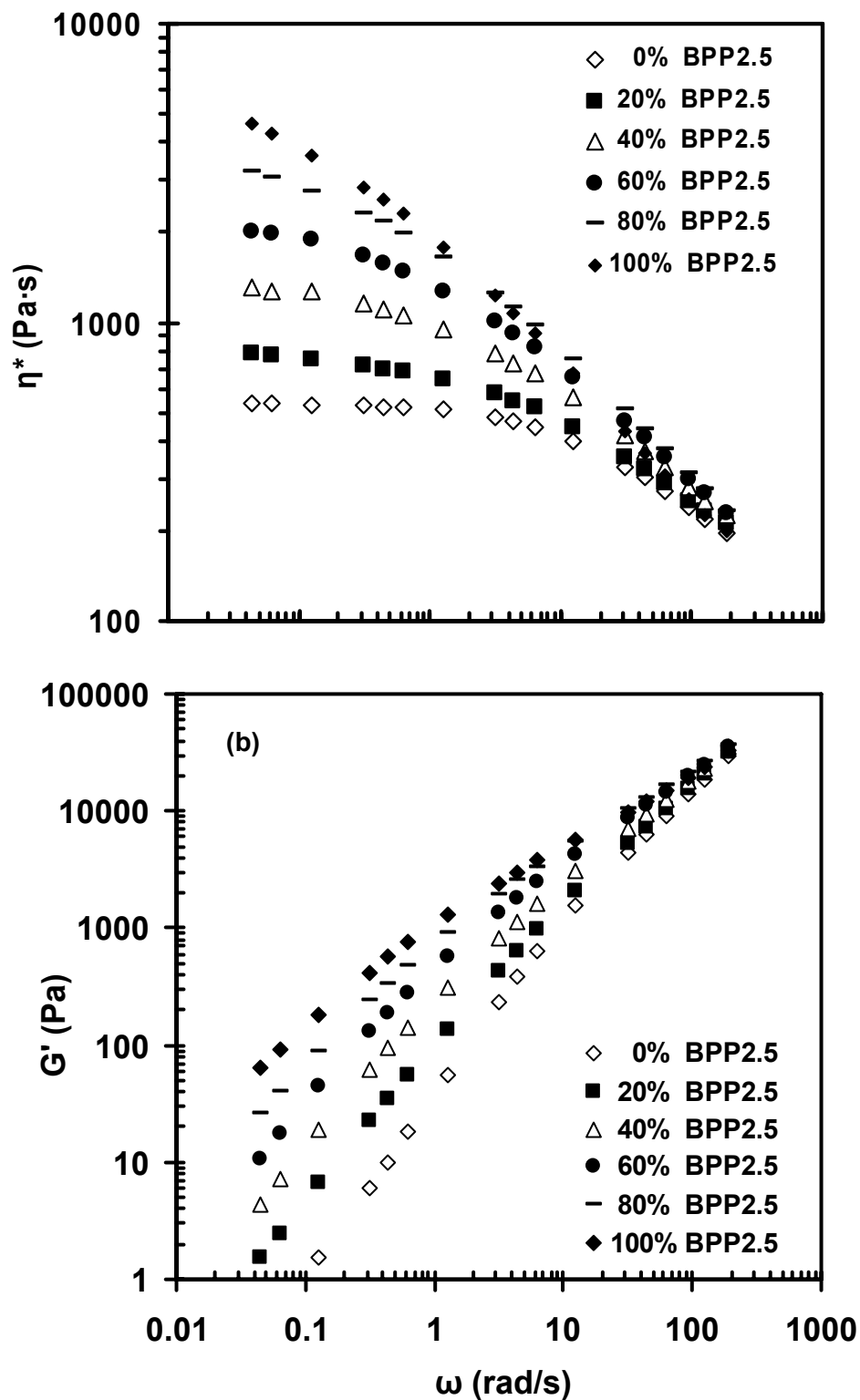


Figure 3.2. (a) Complex viscosities, η^* and (b) elastic moduli, G' , as a function of frequency, ω , for LPP35/BPP2.5 blends at 210 °C.

The Cross model, Equation (1), was applied to the data

$$\eta(\omega) = \frac{\eta_o}{1 + |\lambda\omega|^{(1-n)}} \quad (1)$$

where η is the shear viscosity; η_o is the zero shear viscosity; λ is a relaxation time; n is a constant related to the shear-thinning behaviour; and ω is the frequency, in rad/s. According to the Cross model parameters shown in Table 3.2, increasing the amount of branched PP in the blend results in higher zero shear viscosities and increased relaxation times. The zero shear viscosities, estimated using the Cross model, are plotted as a function of the blend composition in Figure 3.3. These are in good agreement with the zero shear viscosities determined from the creep experiments, also included in Figure 3.3. Both blend systems obey closely the log-additivity rule of viscosity in the melt state. Adherence to the additivity rule has been used as evidence of miscibility of the blend components in the melt state [13].

Table 3.2. Cross and power law model parameters for LPP35/BPP30 and LPP35/BPP2.5 blends.

	Cross		Power Law	
	η_0 (Pa.s)	λ (s)	m (Pa.s ⁿ)	n
<i>LPP35/BPP2.5</i> ¹				
100/0	550	0.02	1589	0.54
80/20	835	0.06	2246	0.51
60/40	1493	0.25	2426	0.50
40/60	2430	0.64	2888	0.48
20/80	4076	1.71	2844	0.49
0/100	7451	8.38	4212	0.44
<i>LPP35/BPP35</i> ²				
100/0	1020	0.02	1589	0.54
80/20	1170	0.04	1695	0.54
60/40	1226	0.06	1787	0.52
40/60	1452	0.08	1722	0.53
20/80	1566	0.14	1837	0.51
0/100	1767	0.21	1735	0.51

¹ From measurements obtained at 210°C

² Cross model and power-law model parameters from measurements obtained at 180°C and 210°C respectively

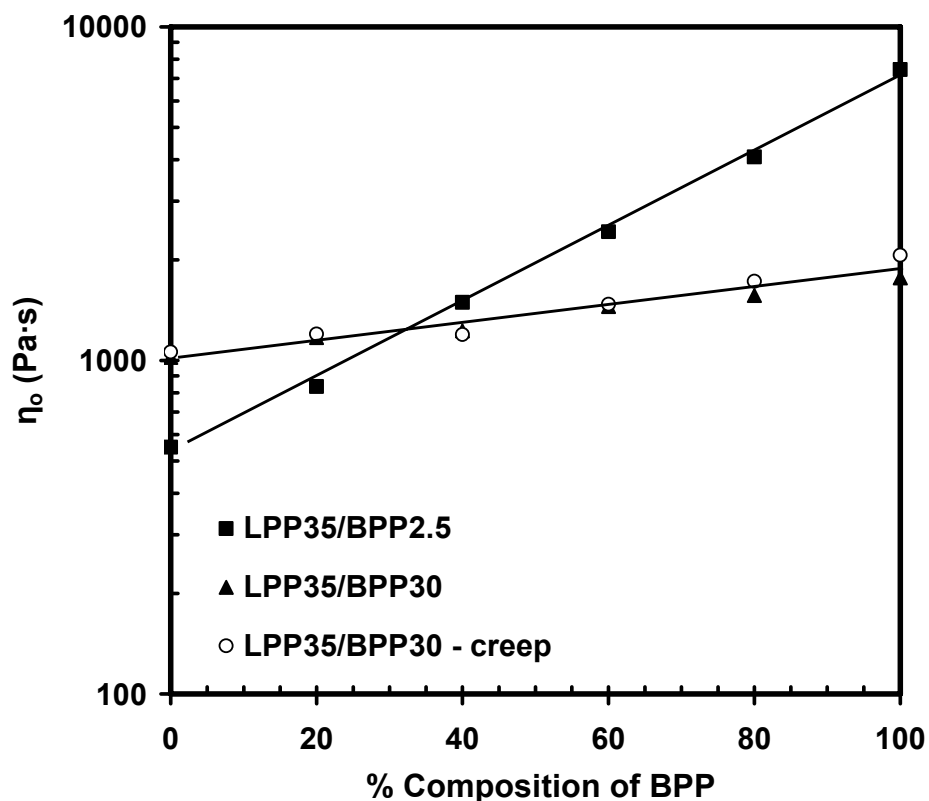


Figure 3.3. Zero shear viscosity of LPP35/BPP2.5 and LPP35/BPP30 blends at 210°C and 180°C respectively. Solid lines denote the log-additivity rule of viscosity.

In a further effort to assess whether these blends are miscible, Cole-Cole plots [23] were constructed. Blends that produce Cole-Cole plots with a semicircular shape are generally considered miscible [9, 14, 24]. Semicircular shapes are evident in Figure 3.4(a) for the LPP35/BPP30 blends and in Figure 3.4(b) at low BPP2.5 contents. The results are not conclusive in the case of the BPP2.5-rich LPP35/BPP2.5 blends, given that the terminal flow regime was not reached within the experimentally accessible range of frequencies (Figure 3.4b).

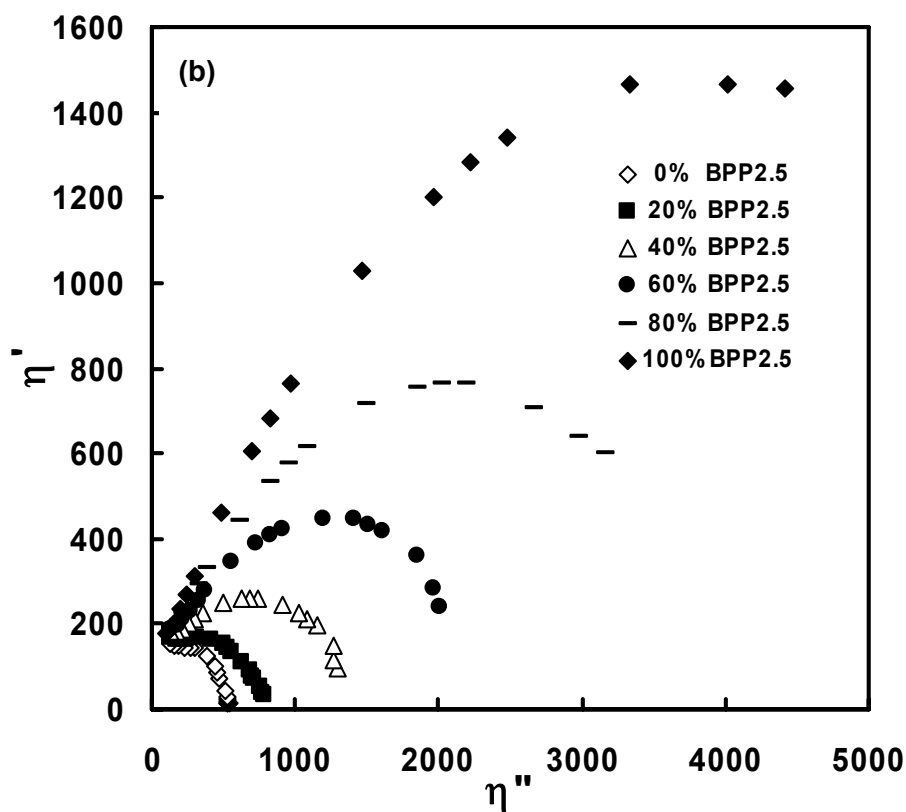
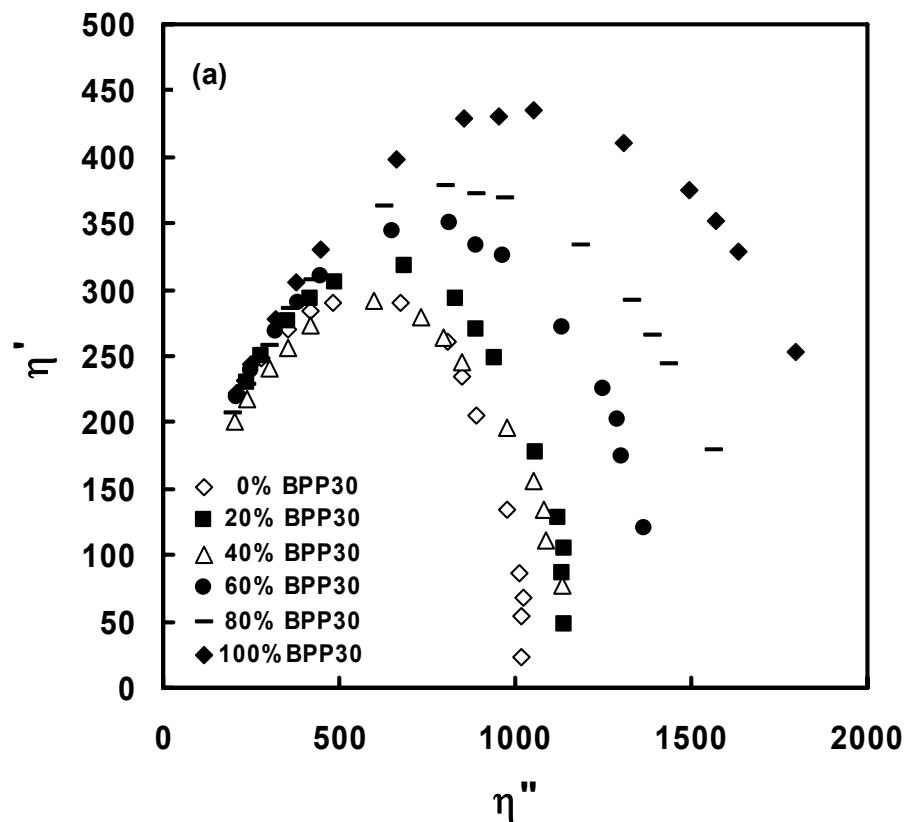


Figure 3.4. Cole-Cole plots of (a) LPP35/BPP30 blends at 180°C, (b) LPP35/BPP2.5 blends at 210 °C.

Weighted relaxation spectra were constructed to extract further information about miscibility of these materials in the melt state [8, 25]. The continuous relaxation spectrum, $H(\lambda)$ was determined by fitting experimental $G'(\omega)$ and $G''(\omega)$ data using Equations (2) and (3) in accordance with the numerical differentiation procedure developed by Ninomiya and Ferry [26].

$$G'(\omega) = \int_{-\infty}^{\infty} H(\lambda) \frac{\omega^2 \lambda^2}{1 + \omega^2 \lambda^2} d \ln \lambda \quad (2)$$

$$G''(\omega) = \int_{-\infty}^{\infty} H(\lambda) \frac{\omega \lambda}{1 + \omega^2 \lambda^2} d \ln \lambda \quad (3)$$

The weighted relaxation spectra, $(\lambda H(\lambda))$ as a function of $\log \lambda$ of the LPP35/BPP30 blends can be seen in Figure 3.5. All the pure components and blend compositions exhibited single peaks; the characteristic relaxation time corresponding to BPP30 was approximately one order of magnitude higher than that of LPP35. Broader relaxation spectra, with higher characteristic relaxation times are expected due to the presence of branching [27, 28]. The smooth transition from the peak of the pure linear PP to the peak of the pure branched PP implies the miscibility of the LPP35/BPP30 blend components. Due to its substantially higher molecular weight, BPP2.5 displays a characteristic relaxation time that is orders of magnitude higher than that of LPP35. Given that the BPP2.5, as well as the BPP2.5-rich blends did not reach the terminal flow region, the relaxation spectra of this set of blends were not meaningful.

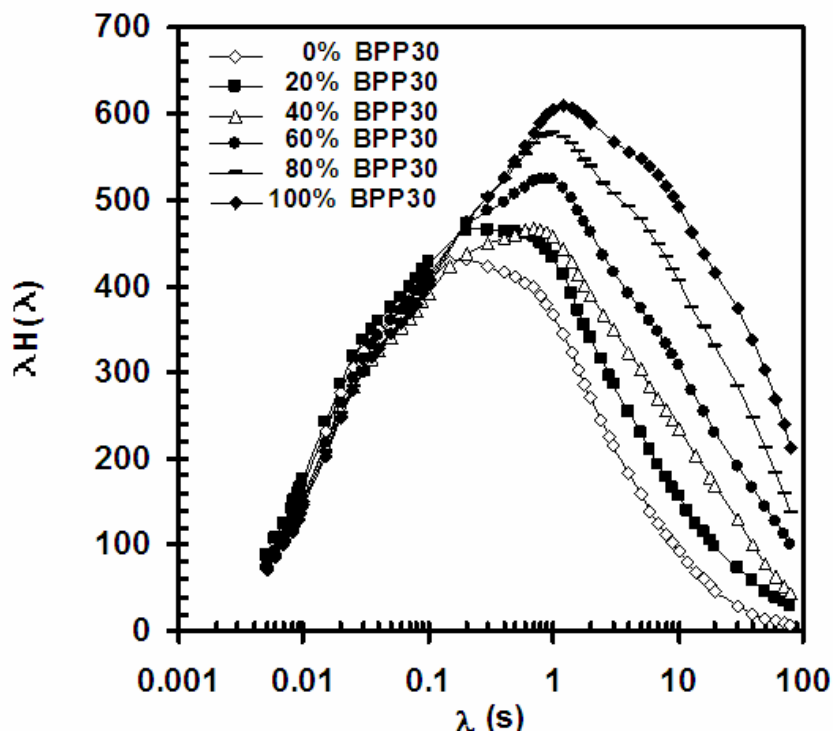


Figure 3.5. Weighted relaxation spectra of LPP35/BPP30 blends at 180°C

3.3.2 Steady Shear Rheology

Figures 3.6 (a) and (b) illustrate the shear viscosities of the LPP35/BPP2.5 and LPP35/BPP30 blends, respectively, as a function of the shear rate. These superimpose well with complex viscosity versus frequency data, obtained from oscillatory experiments at the same temperature, indicating that these blends generally obey the Cox-Merz rule. It should be noted that a slight deviation from the Cox-Merz rule is observed for BPP2.5.

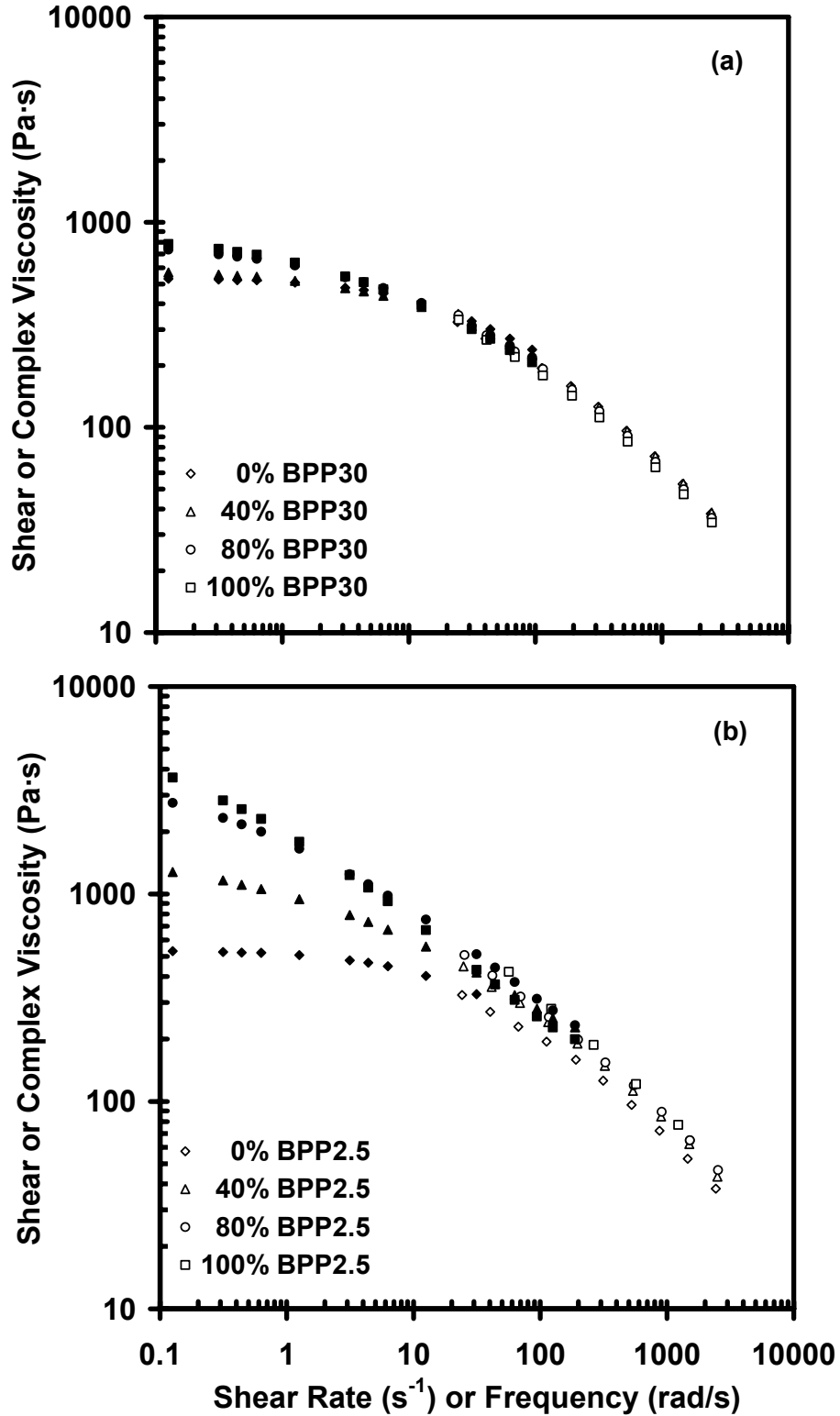


Figure 3.6. Combined shear and complex viscosities as a function of shear rate or frequency at 210°C; (a) LPP35/BPP30 blends; (b) LPP35/BPP2.5 blends. Open symbols denote capillary data, whereas closed symbols represent oscillatory data.

The power law model (equation 4), where m is the consistency index and n is the power-law index was applied to the capillary data. The resulting parameters are summarized in Table 3.2.

$$\eta = m \cdot \dot{\gamma}^{n-1} \quad (4)$$

The properties of LPP35 remain largely unaffected by the addition of BPP30. BPP2.5 has higher viscosity than LPP35 at low shear rates and displays pronounced shear thinning characteristics, due to the presence of long chain branching. The viscosities of the LPP35/BPP2.5 blends are intermediate to those of the pure components.

3.3.3 *Extensional Rheology*

Measurements of the tensile stress growth coefficients versus time, shown in Figures 3.7(a) and (b), provide a characterization of the extensional melt flow behavior of the two series of polypropylene blends. Superimposed with the tensile growth curves in these figures is the LVE shear stress growth plot of $3\eta^+(t)$, which was obtained by using the linear viscoelastic moduli to determine the relaxation spectrum in terms of a discrete spectrum of Maxwell relaxation times. The storage and loss moduli with respect to the discrete Maxwellian spectrum can be expressed as:

$$G'(\omega) = \sum_{i=1}^N G_i \frac{(\omega\lambda_i)^2}{1 + (\omega\lambda_i)^2} \quad (5a)$$

$$G''(\omega) = \sum_{i=1}^N G_i \frac{\omega\lambda_i}{1 + (\omega\lambda_i)^2} \quad (5b)$$

where ω is the frequency of oscillation and G_i and λ_i are the generalized Maxwell model

parameters. The parameters (G_i, λ_i) of Equation (5) were determined using a nonlinear optimization program following the algorithm developed by Baumgärtel and Winter [29]. Employing this program results in the calculation of the least number of (G_i, λ_i) parameters (Parsimonious spectra). The discrete relaxation spectra of (G_i, λ_i) are then used in the following expression:

$$\eta_E^+ = 3\eta^+ = 3 \cdot \sum_i \frac{G_i}{\lambda_i} \left[1 - \exp\left(-\frac{t}{\lambda_i}\right) \right] \quad (6)$$

For the linear PP the agreement of the low-strain tensile portions of the tensile stress growth curves with the shear stress growth plots shown in Figures 3.7(a) and (b) provides an experimental validation of Trouton's law; that is the ratio of extensional to shear viscosity was equal to 3. The higher plateau viscosity corresponding to $3\eta^+$ for the linear polymer provides additional evidence of the linearity of the molecules.

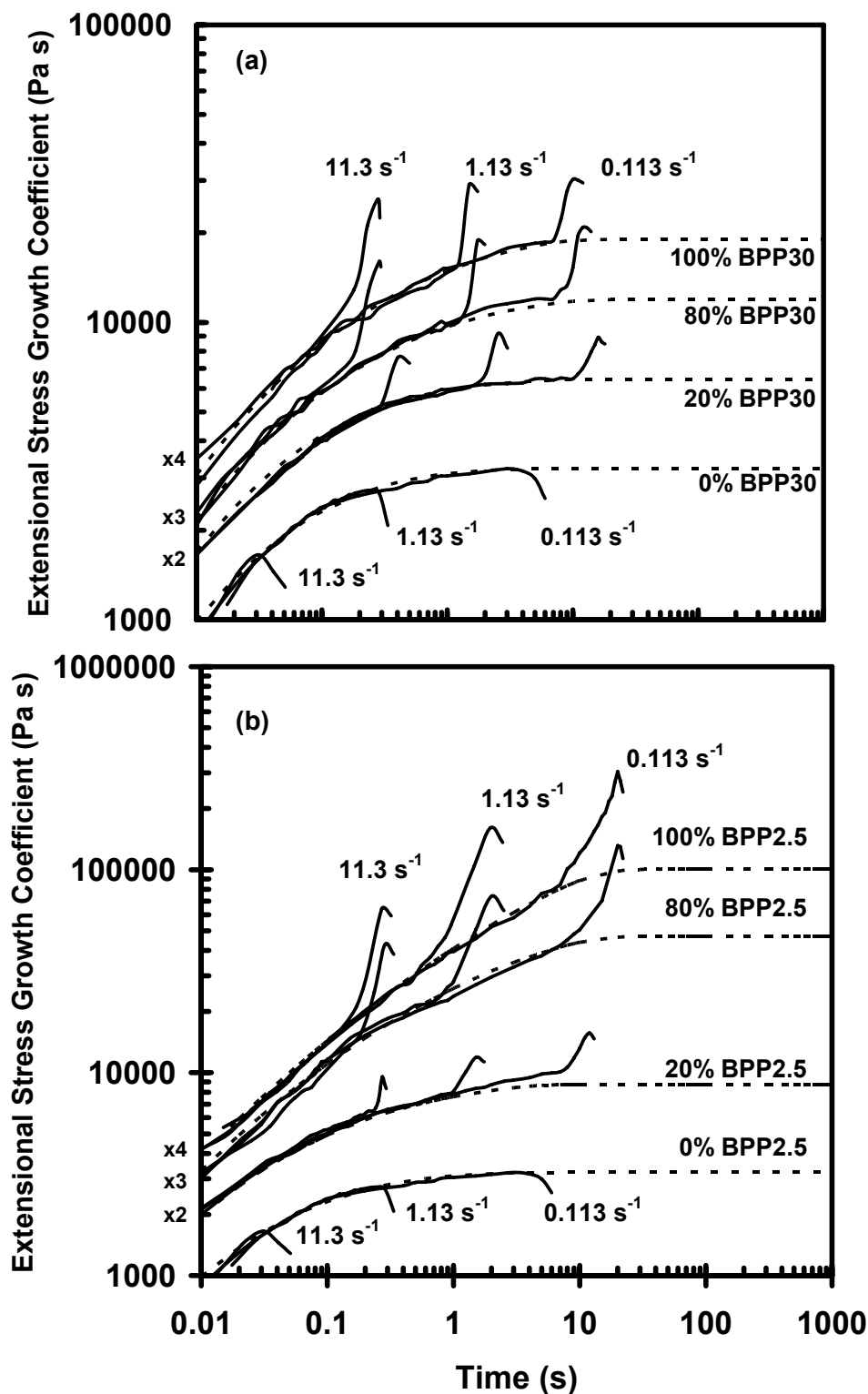


Figure 3.7. Extensional stress growth coefficient rate at 175°C; (a) LPP35/BPP30 blends; (b) LPP35/BPP2.5 blends. Dotted lines denote the LVE shear stress growth coefficient η^+ obtained from a Maxwell model fit, using experimental data obtained from linear oscillatory measurements at 175°C.

Branched PPs display strain hardening, manifested as a deviation from the predicted LVE stress growth behaviour, as expected in long chain branched polyolefins [7, 19, 28, 30, 31]. Significant strain hardening takes place even upon addition of low amounts of branched PP in linear PP, for both series of blends. This behaviour becomes more pronounced as the Hencky strain rate is increased. First the tensile stress growth coefficient rises to higher levels as the amount of the long chain branched PP increases. The sudden decrease taking place subsequently corresponds to failure of the sample. The stress growth coefficient deviates from its linear behaviour at earlier times when the amount of branched PP in the blend is augmented. Similar enhancements in strain hardening have been reported before in PE blends [9-11], as well as linear/branched PP blends [7, 18]. Micic et al. [16] attributed the observed enhancements in melt strength, extensional viscosity and strain hardening of LLDPE/LDPE blends to the immiscibility of the blend components in the melt state. The influence of phase structure on the extensional properties of polyolefin blends has not been addressed extensively in the literature, but the results of the present study suggest that miscible PP blends exhibit strain hardening.

3.3.4 Thermal Properties

All sets of blends exhibit single melting and crystallization peaks. The melting and crystallization points (T_m and T_c , respectively) and crystallinities for both sets of blends are summarized in Table 3.3. The melting points of LPP35/BPP2.5 blends have an almost linear dependence on the composition of the branched PP, with the melting point decreasing as BPP2.5 content increases. This provides further evidence of miscibility of

these blends. Substantial decreases in crystallinity are also noted, with PBPP2.5 having a significantly lower crystallinity than the linear PP. These observations are obviously due to the disruption of the crystalline structure of PP in the presence of long chain branching.

Table 3.3. Thermal and tensile properties for LPP35/BPP30 and LPP35/BPP2.5 blends.

	T_m	T_c	Crystallinity (%)	Strain at yield	Stress at yield	Young's Modulus (MPa)
<i>LPP35/BPP30</i>						
100/0	165.9	111.4	60.7	29.0 ± 2.0	30.2 ± 2.4	327.4 ± 52.0
80/20	163.5	126.0	59.5	22.5 ± 0.8	33.6 ± 0.1	406.3 ± 61.7
60/40	163.9	127.9	60.3	18.6 ± 2.1	35.9 ± 1.5	443.3 ± 24.3
40/60	163.6	127.5	64.9	20.0 ± 0.6	34.9 ± 0.6	415.3 ± 28.2
20/80	163.9	128.5	61.7	22.1 ± 0.1	36.5 ± 0.1	424.0 ± 37.9
0/100	164.1	128.6	62.8	19.1 ± 2.0	36.9 ± 2.4	456.1 ± 53.5
<i>LPP35/BPP2.5</i>						
100/0	165.9	111.4	60.7	29.0 ± 2.0	30.2 ± 2.4	327.4 ± 52.0
80/20	164.1	128.8	53.7	29.9 ± 0.6	29.1 ± 1.4	253.0 ± 0.1
60/40	163.3	129.6	56.7	27.4 ± 1.7	30.6 ± 0.1	307.4 ± 25.8
40/60	162.8	130.1	54.0	23.2 ± 3.1	33.9 ± 0.1	373.4 ± 42.2
20/80	162.0	129.8	52.8	23.1 ± 2.1	33.5 ± 0.6	393.1 ± 10.9
0/100	161.3	129.0	43.2	24.6 ± 2.0	33.5 ± 0.6	374.9 ± 21.7

Note: Error represents the 95% confidence intervals.

The melting points of the LPP35/BPP30 remain virtually unaffected and addition of BPP30 to the blends yields a slight increase in crystallinity. This result was unexpected and it may be due to BPP30 containing lower amounts of long chain branching and/or having a more homogeneous long chain branching distribution.

With respect to the crystallization temperatures, both sets of blends show a dramatic increase upon the addition of a small fraction of branched PP; further additions caused only minimal changes. This trend is similar to previously published results [5].

3.3.5 Mechanical Properties

Table 3.3 displays the tensile properties, including the strain at yield (%), the stress at yield (MPa), and the Young's moduli. For both sets of blends increasing the branched PP content leads to an increased tensile stress and Young's modulus, and a decreased tensile strain.

Flexural properties, including maximum flexural stress and flexural modulus as a function of blend composition, can be seen in Figure 3.8. The flexural moduli of all blends are higher than the linear sample; however, the increase is much more pronounced in the blends containing BPP30.

Overall, all blends exhibit better stiffness than the linear PP. Additionally, the LPP35/BPP30 blends demonstrate better flexural and tensile properties when compared to the LPP35/BPP2.5 system. This trend may be attributed to the higher values of crystallinity exhibited by the LPP35/BPP30 blends.

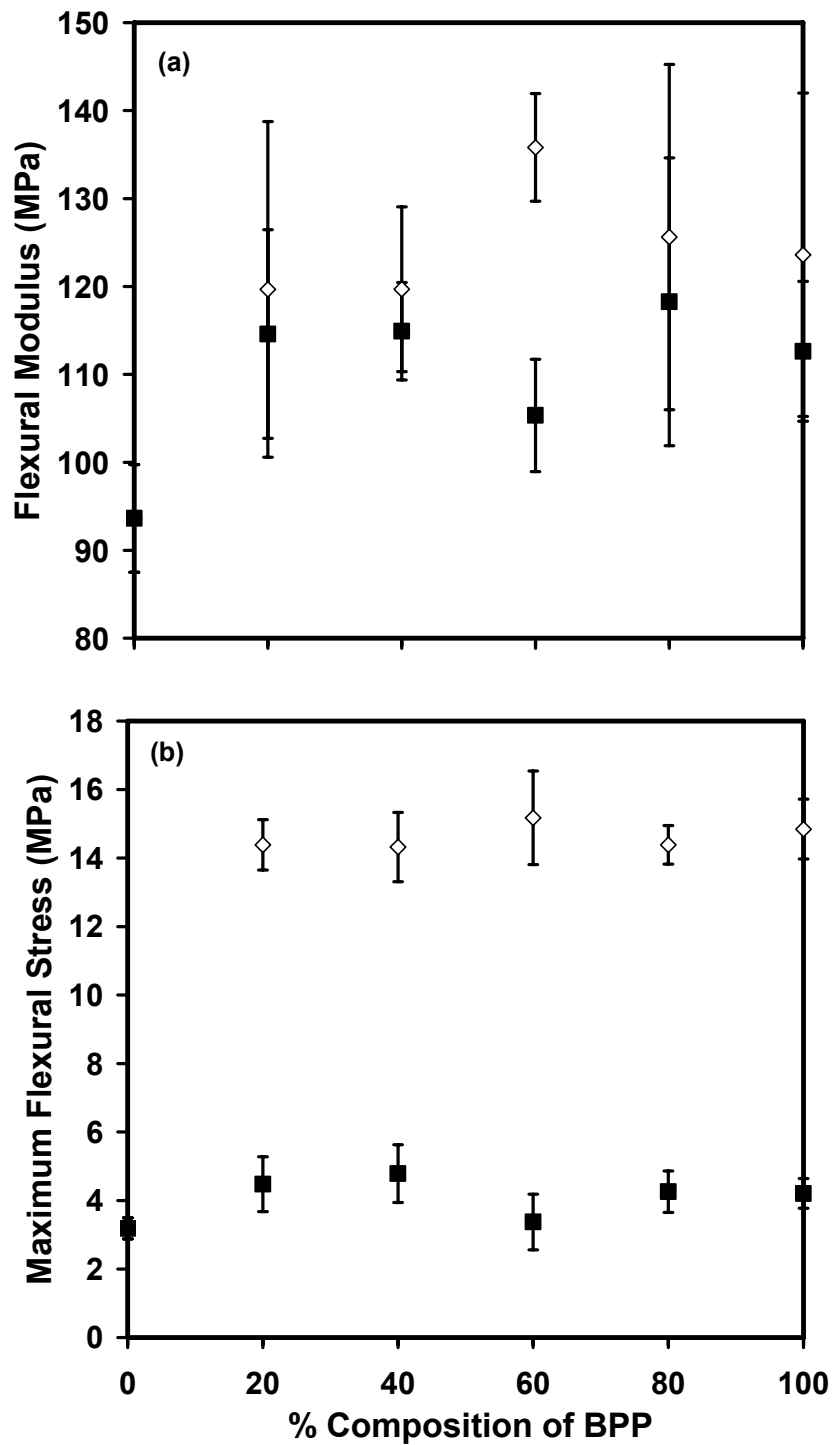


Figure 3.8. (a) Flexural moduli and (b) flexural stresses as a function of BPP content for ■ LPP35/BPP2.5 and ◇ LPP35/BPP30 blends. TPOs, PP blends. Error bars represent 95% confidence intervals.

3.4 Conclusions

Blends of linear and branched PPs exhibited increased melt elasticity and strain hardening, and produced more pronounced shear thinning behaviour. Based on the rheological and thermal characterization, these blends appeared to be miscible.

The melting points and crystallinities were affected substantially upon introduction of the higher molecular weight BPP2.5 resin, whereas they remained virtually unaffected in the presence of BPP30. The crystallization points increased significantly upon addition of low amounts of branched PPs for both sets of blends.

The flexural properties and tensile moduli increased with the introduction of branched PP; the blends containing BPP30 displayed better mechanical properties; this was credited to the higher crystallinity of BPP30.

3.5 References

1. P. Spitael, C.W. Macosko and A. Sahnounne, *Proceedings SPE ANTEC*, 2, 1791 (2002).
2. G.J. Nam, J.H. Yoo and J.W. Lee, *J App Polym Sci*, 96, 1793 (2005).
3. H.E. Naguib and C.B. Park, *Polym Eng Sci*, 42, 1481 (2002).
4. A.D. Gotsis, B.L.F. Zeevenhoven and A.H. Hogt, *Polym Eng Sc.*, 44, 973 (2004).
5. H.E. Naguib, J.X. Xu, C.B. Park, A. Hesse, U. Panzer, and N. Reichelt *Proceedings SPE ANTEC*, 2, 1623 (2001).
6. N. Reichelt, M. Stadlbauer, R. Folland, C.B. Park and J. Wang, *Cell Polym*, 22, 315 (2003).
7. P. Spitael and C.W. Macosko, *Polym Eng Sci*, 44, 2090 (2004).
8. Y. Fang, Carreau, P.J. and P.G. Lafleur, *Polym Eng Sci*, 45, 1254 (2005).

9. K. Cho, B.H. Lee, K.-M. Hwang, H. Lee and S. Choe, *Polym Eng Sci*, 38, 1969 (1998).
10. P. Micic, S.N. Bhattacharya and G. Field, *Intern Polym Process*, XI, 14 (1996).
11. A. Ghijssels, J.J.S.M. Ente and J. Raadsen, *Intern Polym Process*, VII, 44 (1992).
12. C. Liu, J. Wang and J. He, *Polymer*, 43, 3811 (2002).
13. L.A. Utracki and B. Schlund, *Polym Eng Sci*, 27, 512 (1987).
14. H. Kwag, D. Rana, K. Cho, J. Rhee, T. Woo, B.H. Lee and S. Choe, *Polym Eng Sci*, 40, 1672 (2000).
15. F. Chen, R. Shanks and G. Amarasinghe, *J App Polym Sci*, 81, 2227 (2001).
16. P. Micic, S.N. Bhattacharya and G. Field, *Intern Polym Process*, XII, 110 (1997).
17. P. Micic, S.N. Bhattacharya and G. Field, *Intern Polym Process*, XIII, 50 (1998).
18. J. Stange, C. Uhl, and H. Münstedt, *J Rheol*, 49,1059 (2005).
19. J.M. Dealy and K.F. Wissbrum, *Melt Rheology and Its Role in Plastics Processing*, Boston: Kluwer Academic Publishers (1999).
20. M.L. Sentmanat, US Patent 6,578,413 (2003).
21. M.L. Sentmanat, *Rheol Acta*, 44, 657 (2003).
22. M.L. Sentmanat, E.B. Muliawan, and SG Hatzikiriakos, *Rheol Acta*, 44, 1 (2004).
23. K.S. Cole and R.H. Cole, *J Chem Phys*, 9, 341 (1941).
24. L.A. Utracki, *Two Phase Polymer Systems*, L.A. Utracki Ed., New York: Hanser (1991).
25. C. Lacroix, M. Aressy and P.J. Carreau, *Rheo Acta*, 36, 416 (1997).
26. J.D. Ferry, *Viscoelastic Properties of Polymers*, 3rd ed., New York: Wiley (1980).
27. C. Tzoganakis, *Can J Chem Eng*, 72, 749 (1994).
28. A.D. Gotsis, B.L.F. Zeevenhoven, C. Tsenoglou, *J Rheol*, 48, 895 (2004).
29. M. Baumgartel, and H.H. Winter, *Rheol Acta*, 28, 511 (1989).

30. M.L. Sentmanat, B.N. Wang and G.H. McKinley, *J Rheol*, 49, 585 (2005).
31. S. Kurzbeck, F. Oster, H. Münstedt, T.Q. Nguyen and R. Gensler, *J Rheol*, 43, 359 (1999).

CHAPTER 4

Morphology, Properties and Foaming Characteristics of TPOs Based on Blends of Linear and Branched Polypropylene

4.1 Introduction

Thermoplastic Olefin (TPO) blends, produced by combining polypropylene (PP) with different elastomers, are capable of displaying a broad range of properties, from rigid to soft, depending on the PP to elastomer ratio. Generally, the addition of a rubber phase to PP aims at improving its low temperature impact strength and ductility. This usually comes at the expense of the tensile modulus and flexural properties. Both ethylene-propylene rubber (EPR) and ethylene-propylene-diene terpolymers (EPDM) have been used as the elastomeric content in numerous studies. During the last decade polyolefin elastomers (POEs), metallocene or single-site catalyzed ethylene- α -olefin copolymers are increasingly being used as the rubber phase in TPO blends, due to their relatively low molecular weights and thus improved processability compared with EPRs. This characteristic is particularly favourable for impact modifications of low molecular weight PP [1].

Although TPOs are usually produced with linear PP homopolymers or copolymers, recent developments have highlighted interest for TPOs based on branched PPs or mixtures of linear and branched PPs. The addition of long-chain branches onto a PP backbone has been shown to increase the melt strength of the material, therefore improving the foamability and thermoformability of PP [2-5]. The branched structure is

better able to retard cell coalescence, as well as stabilize bubble growth and increase the expansion ratio during foaming [2, 4, 6].

In the previous chapter we have reported the rheological and physical properties of a series of linear and branched PP blends [7]. Given the potential applicability in foaming and thermoforming applications, it is of interest to investigate the properties of TPOs containing these blends as matrices. The aim of this paper therefore is to investigate the morphology and mechanical properties of TPOs containing various amounts of branched PP in their matrix and to assess their processability in foaming applications, using a batch foaming simulation system.

4.2 Experimental

4.2.1 Materials

The PPs used in this study are two PP homopolymers supplied by Basell (Elkton, MD): a linear PP resin, Pro-fax PD702 (LPP) and a high melt strength branched PP resin, Pro-fax PF611. Their detailed properties are shown in Table 3.1.

The metallocene-based ethylene- α -olefin copolymer used in this research is an ethylene-octene copolymer supplied by The Dow Chemical Company (Midland, MI). This material has an MFI (190°C/2.16kg, g/10min) of 30 and a density of 870 kg/m³.

As outlined in the blend preparation section, a series of PP/POE samples (95/5 and 70/30 by weight) were prepared, with the PP matrix including a range of branched PP compositions (LPP/BPP 20/80, 40/60, 60/40, and 80/20 by weight).

4.2.2 Blend Preparation

Blend components were dry-blended with 0.2% antioxidant (Irganox B225 from CibaGeigy). The dry blended formulations were then compounded at 210°C using a Haake PolyLab Rheocord torque rheometer equipped with a Rheomix 610p mixing chamber and roller rotors until the torque profile reached steady state (approximately 6-7 minutes). The Haake was operated at approximately 70% capacity 100 rpm. Smaller quantities of these blends, suitable for foaming experiments, were prepared using a DSM Xplore 5 ml twin-screw micro-compounder, equipped with a conical co-rotating intermeshing twin-screw element for approximately 5 minutes. All compounding took place under a nitrogen blanket to limit PP degradation.

4.2.3 Rheological Characterization

The viscosity of the blends was measured at a shear rate range of (20-2000 s⁻¹), using a Rosand RH2000 twin bore capillary rheometer (Malvern Instruments) at 210°C. The shear viscosities were calculated by applying the Bagley and Rabinowitch corrections.

The viscoelastic properties were also characterized in the shear oscillatory mode, using a controlled stress rheometer (ViscoTech by Rheologica) equipped with parallel plates 20 mm in diameter. The measurements were performed at a gap of 0.5 mm and a temperature of 180°C, under nitrogen blanket. Samples used in the rheometer were compression molded discs approximately 2 mm in thickness and 25 mm in diameter and were prepared using a Carver hydraulic press, heated at 200°C.

4.2.4 Scanning Electron Microscopy

A JEOL JSM-840 scanning electron microscope was used to characterize the morphology of the blends. Compression molded samples were freeze-fractured under liquid nitrogen, etched in toluene for two hours. The fracture surfaces were sputtered with gold prior to viewing under the microscope.

4.2.5 Thermal Properties

Thermal properties of the blends were analyzed using a TA Instrument DSC Q100. Approximately 5-8 mg of the samples were sealed in aluminum hermetic pans, and subsequently heated from 30°C to 200°C at a rate of 5°C/min. After 10 minutes of isothermal treatment to destroy any residual nuclei, the samples were then cooled at 5°C/min. A second heating sequence performed at 5°C/min allowed for the attainment of the melting temperatures and heats of fusion.

4.2.6 Mechanical Properties

Compression molded sheets were prepared using a Carver hydraulic press, heated to 200°C, and type V specimens were then stamped out of the sheets, according to the ASTM D638 standard. An Instron Universal Tester, model 3369, was used to determine the tensile properties of all the materials. Five replicate runs at a crosshead speed of 50 mm/min were completed at each composition to ensure the reproducibility of the results. Results are reported with their 95% confidence intervals.

Flexural tests were also performed using the Instron 3369, in accordance with ISO 178, at a strain rate of 5 mm/mm/min. The samples having dimensions 80x10x4mm were compression moulded at 200°C with the hydraulic press. The flexural modulus as well as flexural stresses and strains were calculated from the resulting curves.

The impact strength of the blends was tested using an Instron Izod impact testing apparatus, equipped with a 3.95 kg hammer at both at room temperature and -20°C. Samples tested at low temperatures were conditioned in a freezer overnight. Notched specimens were prepared and measurements were performed according to ASTM D256. Tests were repeated 3 times for each experimental condition.

4.2.7 Batch Foaming Experiments

Foaming experiments were conducted using a batch foaming simulation system [8, 9]. The temperature and pressure in the simulation chamber were regulated using a thermostat and a syringe pump, respectively. An ADAC board was used to record the pressure drop during experimentation, while a high speed CCD camera was used to record the foaming behaviour.

Thin disc-shaped samples were prepared by compression molding using a Carver hydraulic press, heated at 200°C. Samples were then placed into the simulation chamber, and the chamber was set to 180°C, under a pressure of 2000 psi, using nitrogen as the blowing agent. A conditioning time of 20 minutes was given to ensure the nitrogen fully saturated the sample. A program based on Labview was used to open the solenoid valve and record the pressure decay, while simultaneously, the CCD camera recorded the bubble behaviour. These simulations were done on the linear/branched PP blends, as

well as their corresponding TPOs containing 30 wt% POE. For each condition, three separate experiments were run, and the images were analyzed using Sigma Scan Pro 5.0 image analysis software. Averages of these runs are reported with their standard deviation.

The pressure drop rate for all experiments was 33 MPa/s. Due to the fact that the pressure drop rate is not constant during batch foaming simulations, this rate refers to the maximum pressure drop rate value. The actual pressure versus time profile is shown in Figure 4.1.

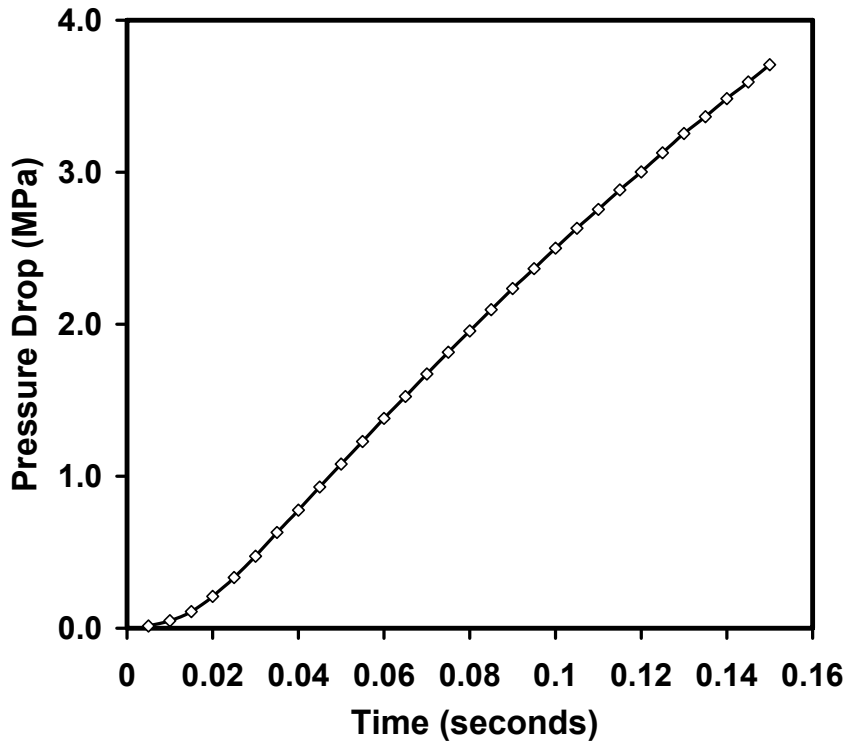


Figure 4.1. Typical pressure drop profile during the batch foaming simulations.

4.3 Results

4.3.1 *Blend morphology*

We first began by an examination of the morphological characteristics of the blends as it is well known that morphology influences the mechanical properties and possibly the foaming behaviour of blends. We investigated the morphology of the blends containing low amounts of the dispersed phase (5 wt% POE), where droplet breakup should be the dominant mechanism, as well as at higher loadings (30 wt% POE), where both particle breakup and coalescence take place. As shown in Figure 4.2 (a) and (b), the addition of branched PP does not affect substantially the morphology of the blends containing 5 wt% POE. The average particle size diameter for these samples was 0.13 μm , irrespective of the branched PP content, This is not surprising, given the similar shear viscosities of the linear/branched PP matrix, irrespective of composition, as shown in Figure 4.3. The addition of branched PP affects the elasticity of the matrix as well, as reported earlier in Chapter 3 but this apparently did not affect particle breakup at low dispersed phase contents, at least at the shear rates relevant to compounding in this work.

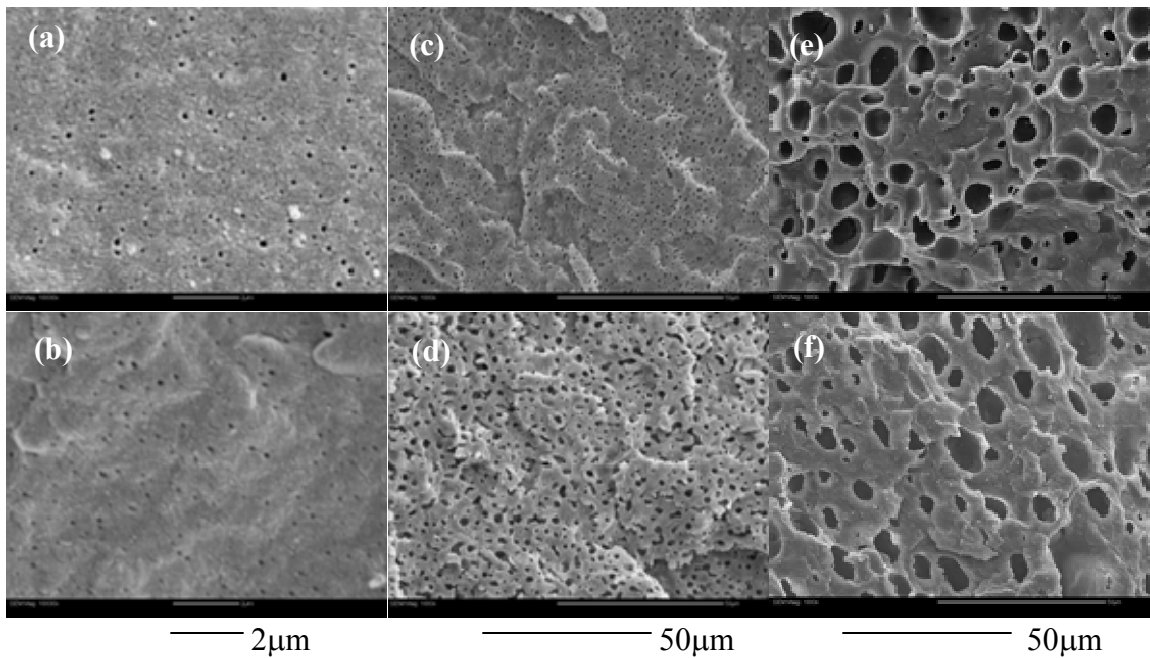


Figure 4.2. SEM images as a function of LPP/BPP/POE wt% composition for: (a) 95/0/5 and (b) 0/95/5 blends prepared in the DSM at 10000x magnification, (c) 70/0/30 and (d) 0/70/30 blends prepared in the DSM at 1000x magnification, and (e) 70/0/30 and (f) 0/70/30 blends prepared in the Haake at 1000x magnification.

Closer inspection of the SEM images of the blends containing 30 wt% POE (Figures 4.2(c) and (d)) reveals that in the presence of branched PP the particles became more irregular. Given that at this POE composition, particle coalescence also plays an important role, this implies that the more elastic matrix may enhance the coalescence rate.

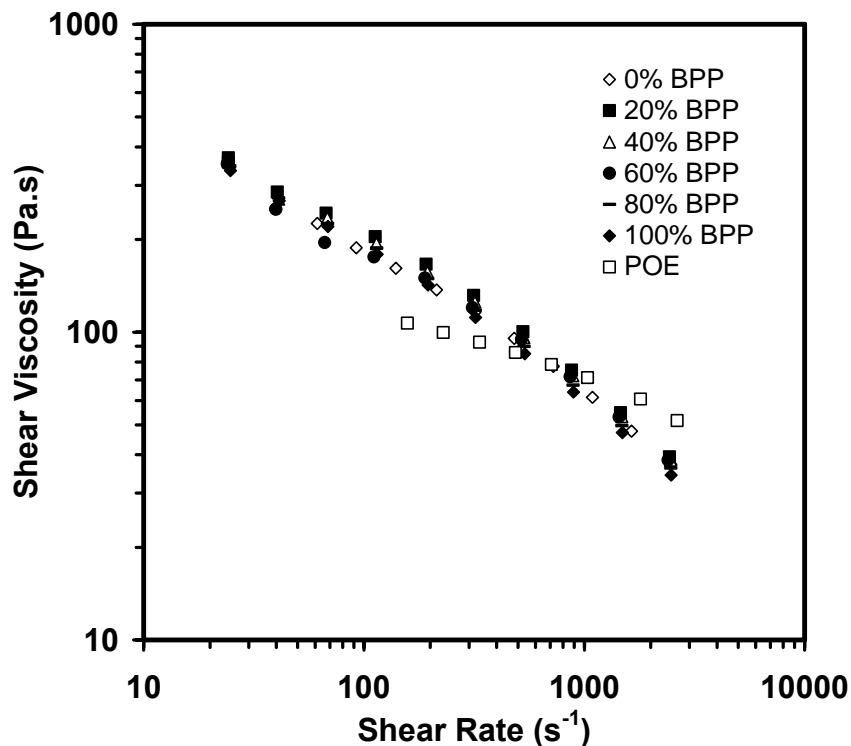


Figure 4.3. Shear viscosity as a function of shearing rate for blends containing various amounts of BPP, and for the virgin POE at 210°C.

The processing method also plays a dominant role, given that the 30 wt% POE blends prepared in the batch mixer (Figures 4.2(e) and (f)) showed average particle size diameters of $1.589 \pm 0.280 \mu\text{m}$, which is substantially higher than the sub-micron size of $0.532 \pm 0.017 \mu\text{m}$ obtained for the same blends with the micro-compounder, which offers a more intensive shear environment.

Given the importance of interfacial tension on the morphology and the properties of immiscible polymer blends, it is also of interest to investigate whether addition of branched PP alters the interfacial tension between the PP matrix and the elastomer dispersed phase. It should be noted that our previous work on linear/branched PP blends (Chapter 3) has revealed that the blend under consideration in this work is miscible in the melt state; therefore the PP matrix should behave as a single phase system. The

interfacial tension was estimated by fitting the Palierne emulsion model [10, 11] to the viscoelastic data obtained through oscillatory shear measurements, for the simplified case where the polydispersity, dv/dn , of the dispersed droplets is less than 2 [11]. A representative illustration of the Palierne model fit for a TPO containing 30 wt% POE as the dispersed phase, with the matrix containing 70/30 LPP:POE is shown in Figure 4.4. The interfacial tension values obtained from these fits are very low, in agreement with previous findings, [1] suggesting excellent compatibility between the PP and POE phases. Specifically, the TPOs containing 100% linear PP in their matrix had an interfacial tension of 0.103 mN/m, whereas those containing 100% branched PP arrived at a value of 0.072 mN/m. All other compositions fell in-between.

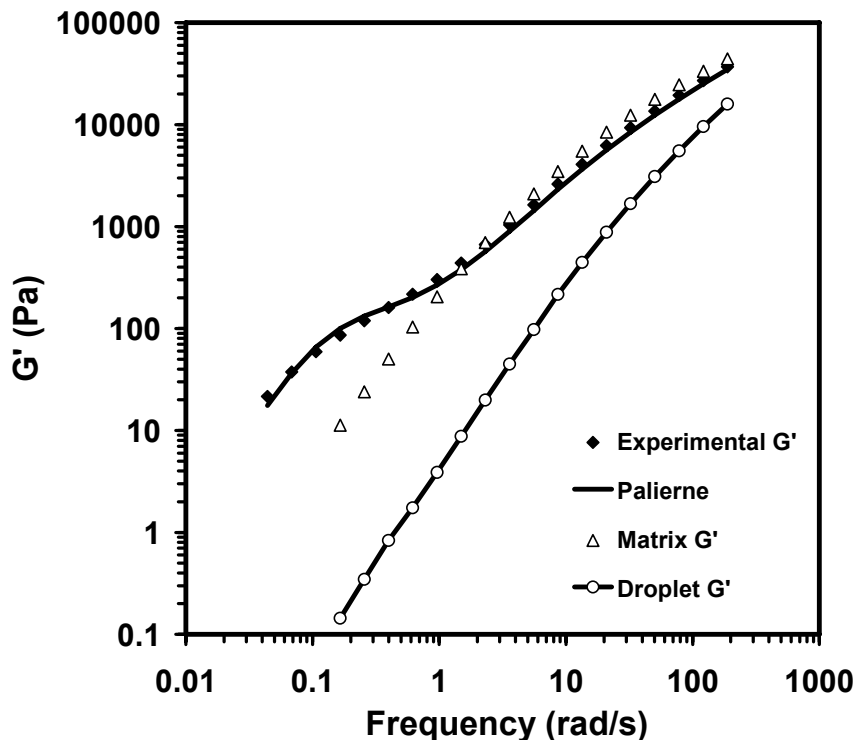


Figure 4.4. Representative fit of the Palierne model for 70/30 wt% LPP/POE blends prepared in the DSM.

4.3.2 Mechanical Properties

As expected, the addition of 30 wt% of POE in the PP matrix decreased substantially the tensile (Young's) modulus of the material (Figure 4.5(a)). At the same time, the elongation at break increased substantially, as the PP matrix displayed elongations below 30%, whereas all the TPOs had elongations at break above 100% (Figure 4.5(b)).

What is more noteworthy is that the trends reported for linear/branched PP blends in the previous chapter; whereby small additions of branched PP generated a stiffer material, persist in the TPOs, as shown in Figure 4.5(a). This is also reflected by the flexural properties in Figure 4.6, which demonstrate that all materials containing branched PP are generally more rigid. Given that there are no notable differences in the morphology and the interfacial tension of the blends, this behaviour is attributed to the increase in the crystallinity of the blend, in the presence of small amounts of the more crystalline branched PP, as shown in Figure 4.7.

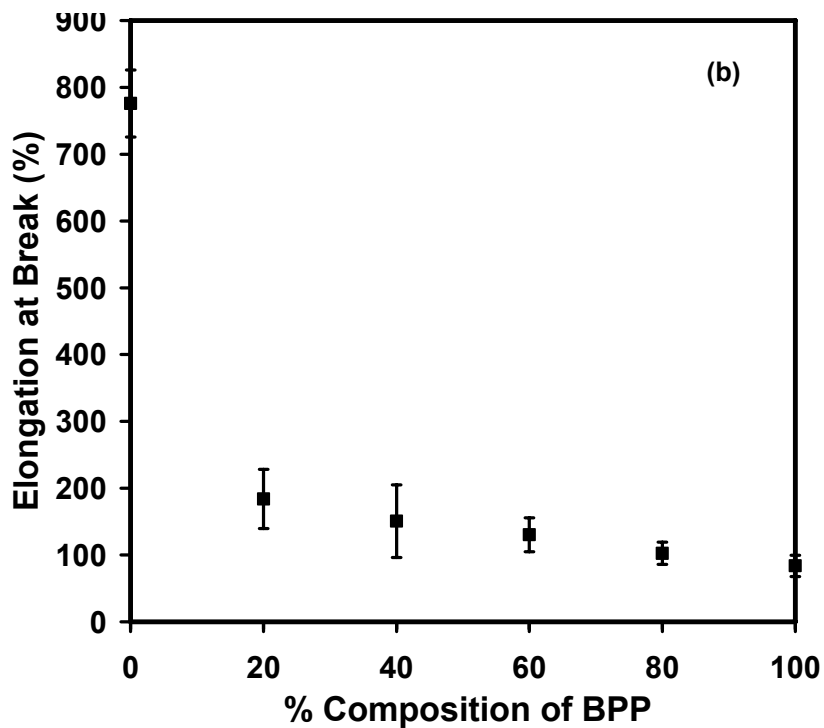
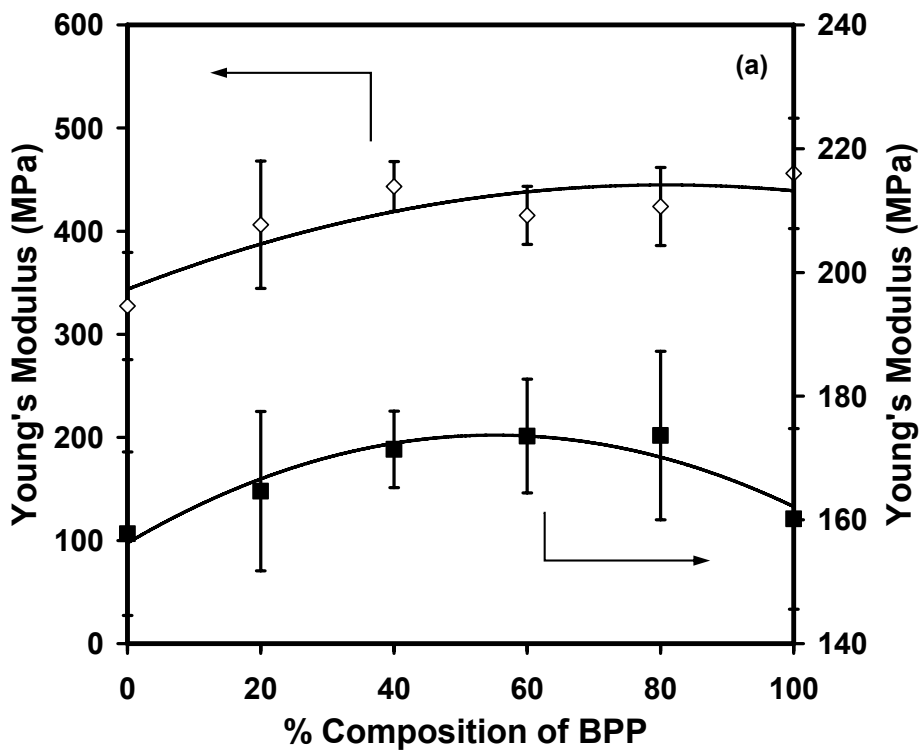


Figure 4.5. (a) Young's moduli and (b) elongation at break as a function of BPP content; ■ TPOs, ◇ PP blends. Error bars represent 95% confidence intervals. Lines are drawn to guide the eye.

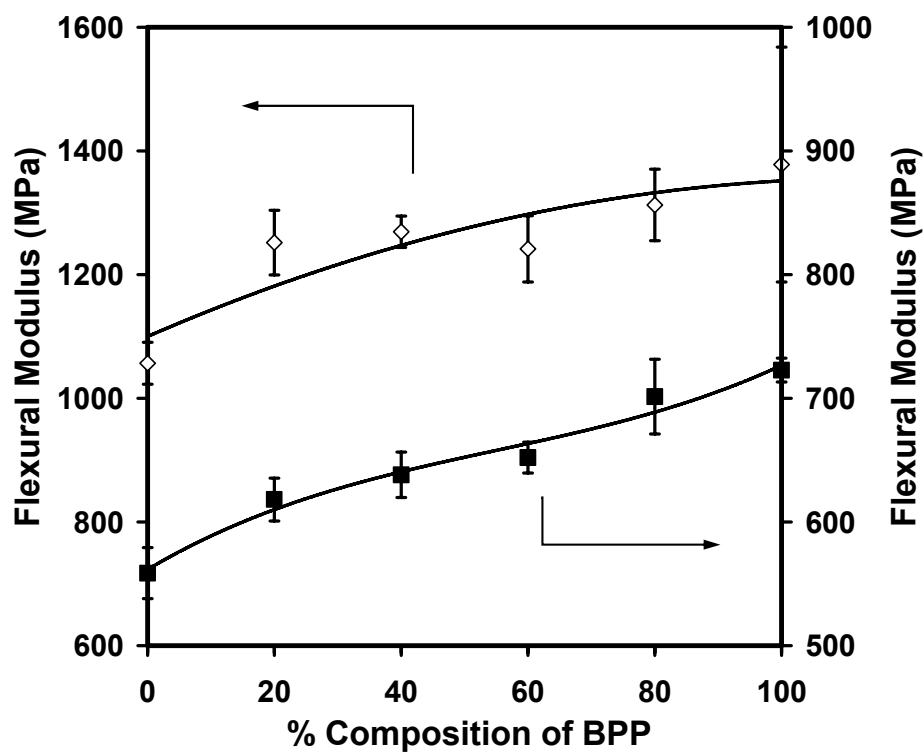


Figure 4.6. Flexural modulus as a function of BPP content; ◇ PP blends, ■ TPOs. Lines are drawn to guide the eye. Error bars represent 95% confidence intervals.

The beneficial effect on stiffness comes at the expense of the elongation at break, as shown in Figure 4.5(b). Nevertheless, of all the blends prepared in this study, none failed during notched Izod impact tests conducted at ambient temperature, whereas at -20°C , the TPO sample containing only branched PP as the matrix failed with an impact energy of 0.011J/m^2 . This confirms that all the materials have good toughness, even at low temperatures.

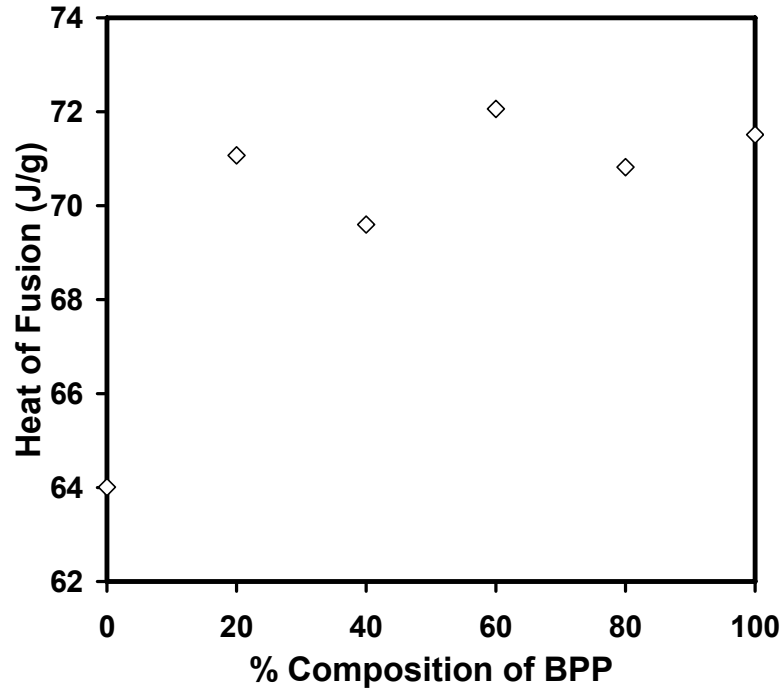


Figure 4.7. Heat of fusion as a function of BPP content for the TPO blends.

4.3.3 Batch Foaming Experiments

Representative images captured during batch foaming of TPOs containing 30 wt% POE can be seen in Figure 4.8.

The cell densities with respect to the unfoamed volume (N_{unfoam}) are determined from [8]:

$$N_{\text{unfoam}}(t) = \left(\frac{N(t)}{A_c} \right)^{\frac{3}{2}} \times \text{VER}(t) \quad (1)$$

where the volume expansion ratio (VER) is:

$$\text{VER}(t) = 1 + \left(\frac{4}{3} \pi (R_{\text{avg}}(t))^3 \times N(t) \right) \quad (2)$$

where $N(t)$ is the number of bubbles observed, A_c is the analysis area, and R_{avg} is the average radius of the observed bubbles.

In the case of the batch foaming simulations, the observations are made only for the initial growth stage, and therefore the VER is approximately equal to 1. Hence, expression for N_{unfoam} can be reduced to:

$$N_{unfoam}(t) = \left(\frac{N(t)}{A_c} \right)^{\frac{3}{2}} \quad (3)$$

The representative cell density versus time curves calculated by image analysis, corresponding to the images of Figure 4.8, calculated by using Equation (3) are shown in Figure 4.9.

Figures 4.10(a) and (b) depict the bubble growth as a function of time for the various blends and Figures 4.11 and 4.12 summarize the final cell density of the foams and the cell density growth rate. The latter was calculated by determining the initial slope of the cell density versus time figures, as functions of the branched PP composition.

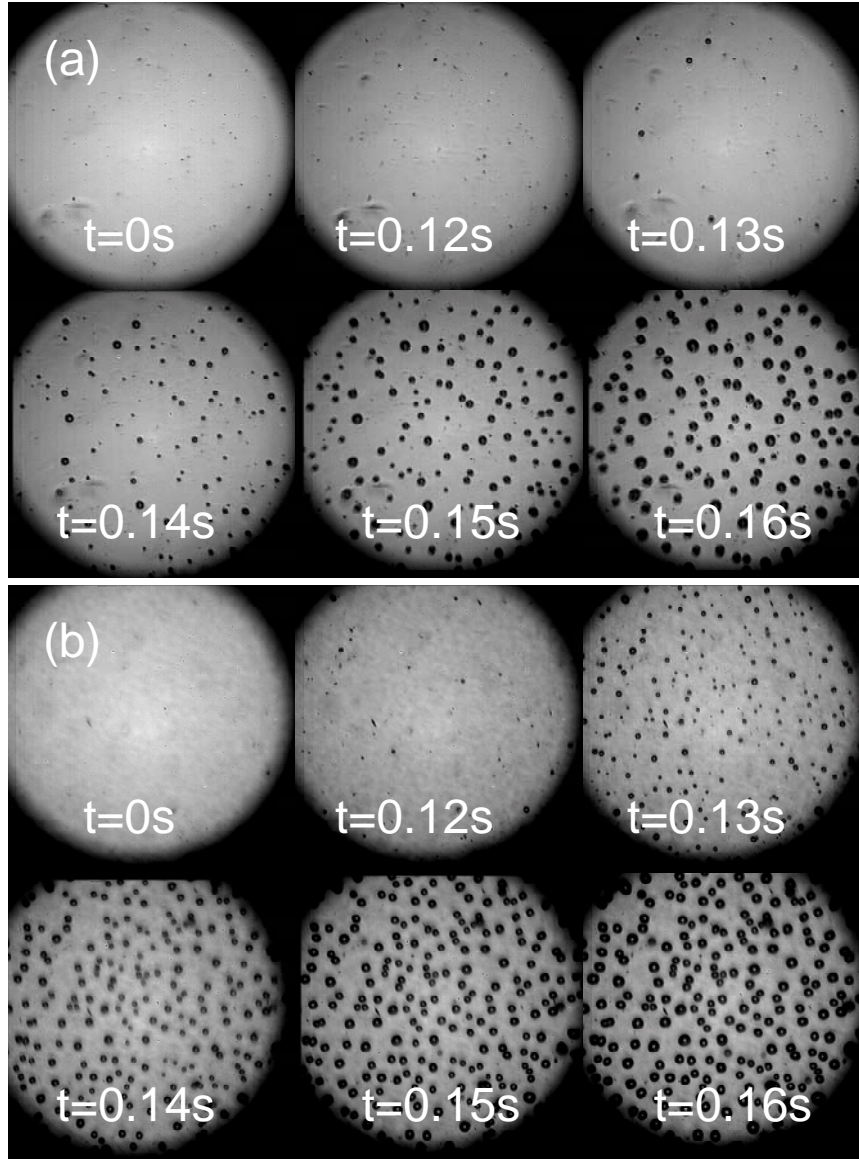


Figure 4.8. Images captured during the batch foaming process of blends containing 100 wt% branched PP and (b) 100 wt% branched PP with 30% POE from 0 to 0.16 seconds using nitrogen as the blowing agent, $P_{\text{sat}} = 2000\text{psi}$, 180°C , $dP/dt=33\text{MPa/s}$.

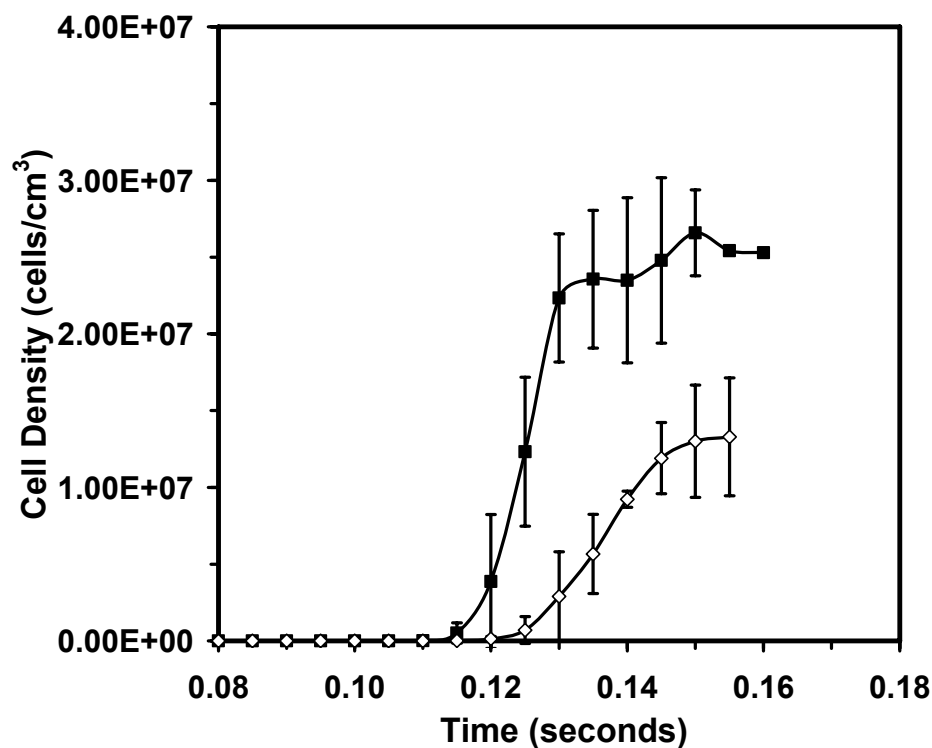


Figure 4.9. Cell density as a function of time; ◇ 100 wt% branched PP blend, ■ 100 wt% branched PP TPO.

As seen in Figures 4.10(a) and (b), the rate of cell growth of the various blends is not significantly different. The differences seen in the nucleation time may be due to the presence of impurities in the samples that might speed up the nucleation in some cases. These results indicate that the increased branched PP content of the blend generally did not affect positively the cell growth rate, in agreement with the findings of Otsuki and Kanai [12], who indicated that the growth rate correlates with the high-frequency elastic modulus data, which in the case of our PP blends are very similar (Figure 3.1).

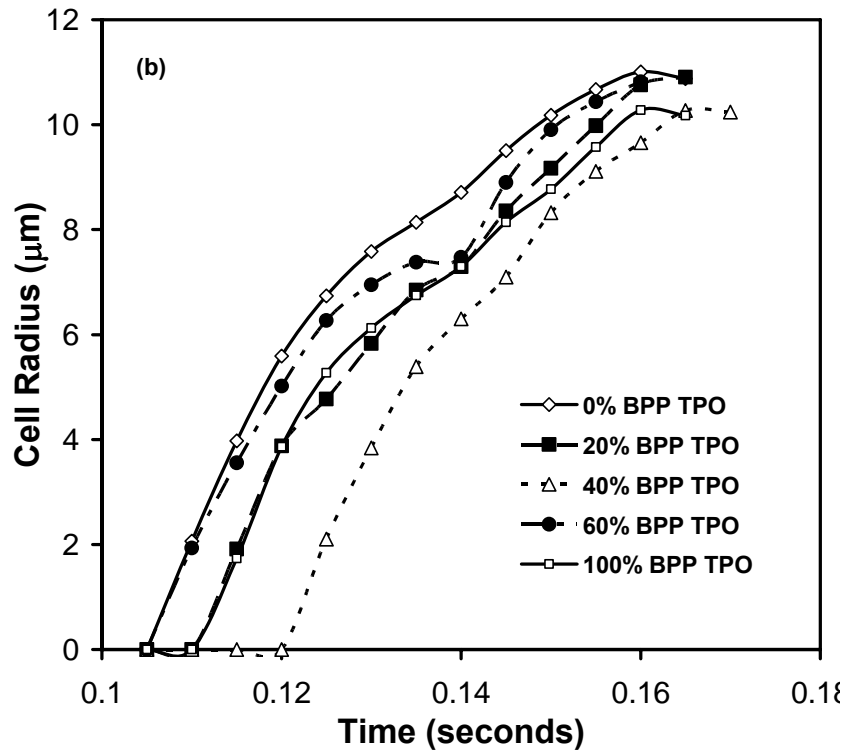
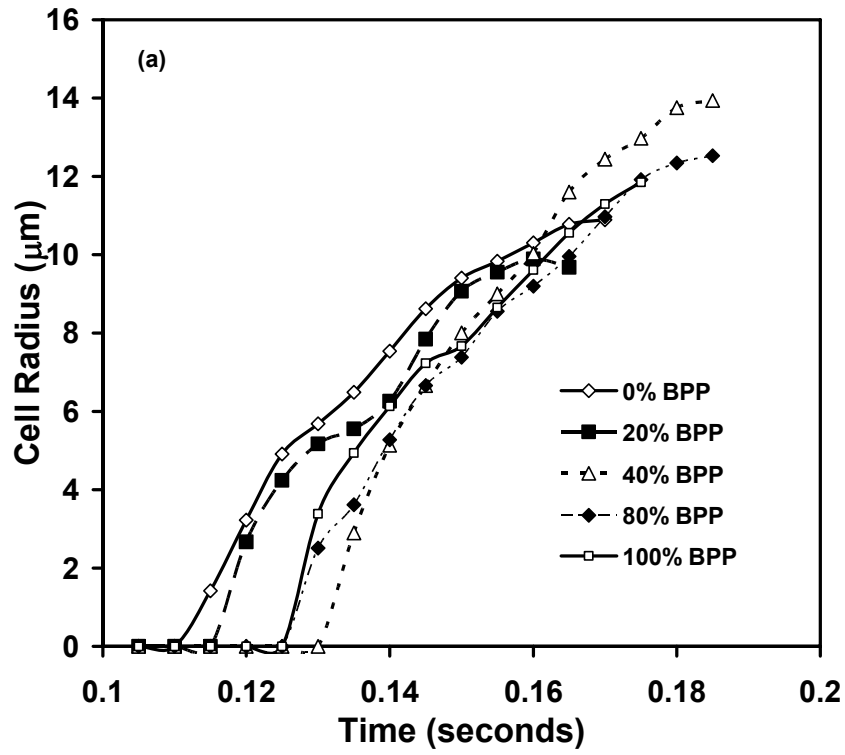


Figure 4.10. Cell radius as a function of time for 10 randomly selected bubbles for (a) PP matrix blends and (b) TPO blends.

Introduction of branched PP actually results in a reduction in the cell growth rate and final cell density, as shown in Figures 4.11 and 4.12. According to Spitael and Macosko [3], linear PP generally nucleates more cells, whereas strain hardening in the branched PPs reduces coalescence. The morphology of the final foams therefore depends on the balance between the two mechanisms. This balance dictates the existence of optimum compositions of branched PP.

It is known that the solubility of the blowing agent in linear PP is higher than that in branched PP [13]. Therefore, it is expected that the blends with a high linear PP content will have higher nuclei density in batch foaming experiments, where a constant pressure is used. Since cell coalescence was not observed in the conducted batch foaming experiments, the final cell density is expected to have the same trend as the cell nuclei density. However, the actual observed cell densities for the 40/60, 60/40 and 80/20 linear PP/branched PP blends showed much lower values than expected. Further studies need to be conducted to clarify these phenomenon.

With respect to the TPO foams, the cell morphology was rather insensitive to the linear PP/ branched PP ratio. It is known that the TPO foams are very sensitive to the amount, morphology and properties of the rubber phase [14]. However in our materials these factors did not change significantly as shown in section 4.3.1.

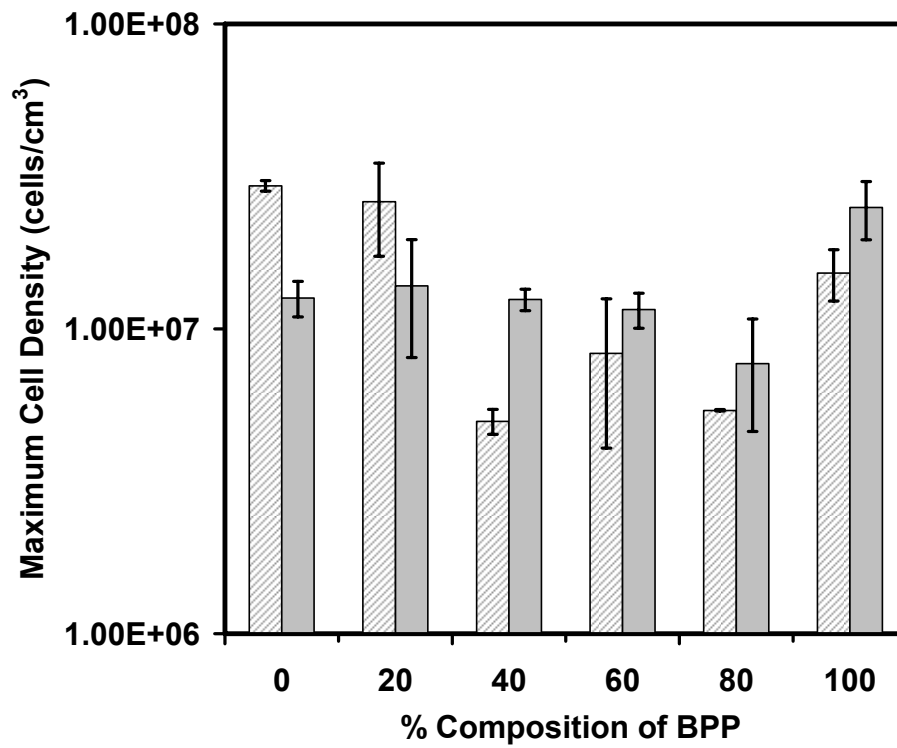


Figure 4.11. Maximum cell density and as a function of BPP content for PP blends, TPOs.

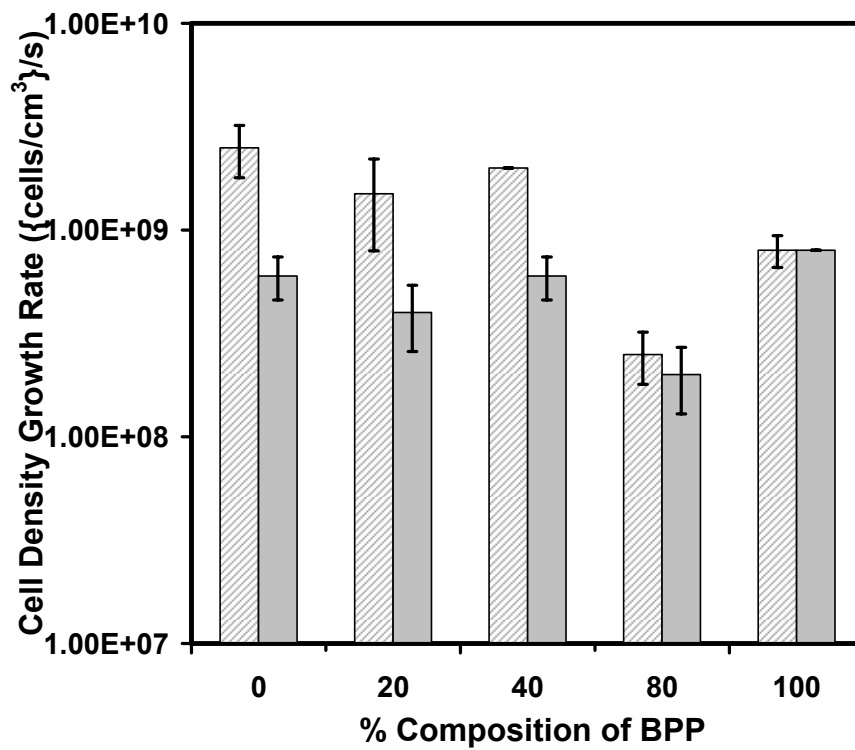


Figure 4.12. Cell growth rate as a function of BPP content for PP blends, TPOs.

Other factors, such as the diffusion coefficient [9, 12], which is influenced by the presence of branching in a polymer melt, probably govern the bubble growth in the linear/branched PP blends under consideration and must be the topic of future investigation. Rheological properties, such as strain hardening most likely affect the final stage of bubble coalescence [15], which is not possible to quantify using the batch foaming simulation apparatus.

Finally, as shown in Figure 4.13, there is no particular trend with regards to the maximum cell radius. Microcellular foams, with cell radii less than 10 μm were produced in all cases. It should be pointed out however that the bubble sizes of the TPO foams show a much larger polydispersity. This is probably due to the presence of two distinct, immiscible components, each one with different foaming characteristics. It is well known that foams made of immiscible polymer blends can result in complex morphologies [16-18]. Distinctly different cell sizes, resulting in a bimodality of the cellular structure have been reported previously by Taki et al. [19] in poly(ethylene-glycol)/polystyrene blends.

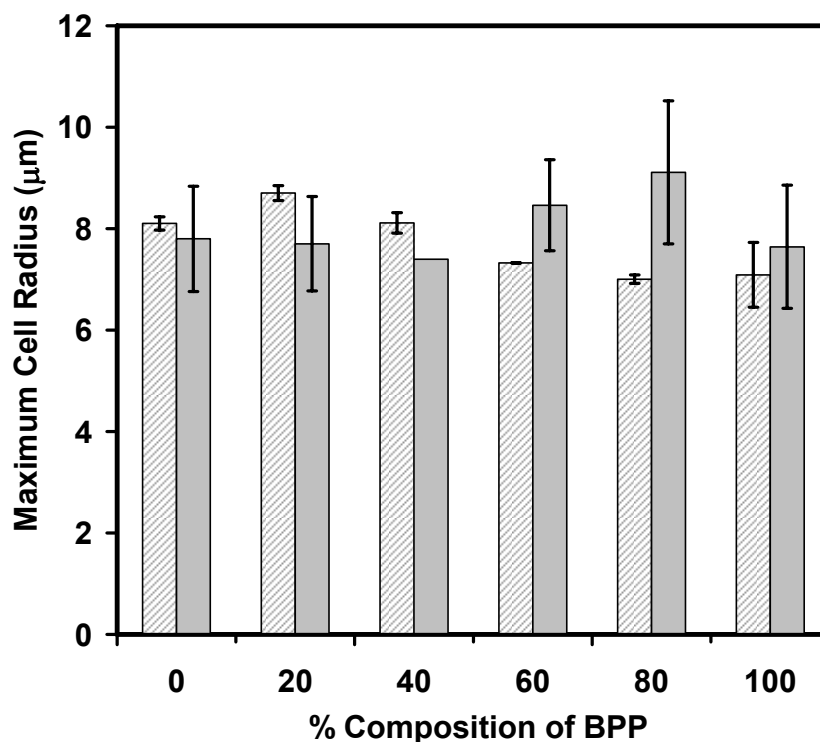




Figure 4.13. Maximum cell radius as a function of BPP content for  PP blends,  TPOs

4.4 Conclusions

Addition of branched PP in TPOs does not alter significantly the morphology or the interfacial tension between the blend components, although some coarsening is seen at high POE contents, possibly due to an increase in the coalescence rate in the presence of a more elastic matrix.

All materials containing branched PP are generally more rigid and have enhanced flexural properties, accredited to the increase in the blend crystallinity. However, these qualities come at the expense of the elongation at break, although even at low temperatures, all blends show good toughness.

Foaming experiments performed using a batch foaming simulation apparatus indicated that the addition of branched PP did not affect substantially the rate of bubble growth in the TPOs and blends containing amounts of 40-80% branched PP showed slower cell growth rates and decreased cell densities.

4.5 References

1. M. Kontopoulou, W. Wang, T.G. Gopakumar, and C. Cheung, *Polymer*, 44, 7495 (2003)
2. G.J. Nam, J.H. Yoo and J.W. Lee, *J App Polym Sci*, 96, 1793 (2005).
3. P. Spitael and C.W. Macosko, *Polym Eng Sci*, 44, 2090 (2004).
4. H.E. Naguib, C.B. Park, U. Panzer and N. Reichelt, *Polym Eng Sci*, 42, 1481 (2002).
5. C.B. Park and L.K. Cheung, *Polym Eng Sci*, 37, 1 (1997).
6. P. Spitael, C.W. Macosko and A. Sahnounne, *Proceedings SPE ANTEC*, 2, 1791 (2002).
7. T.J. McCallum, M. Kontopoulou, C.B. Park, E.B. Muliawan, and S.G. Hatzikiriakos, *Polym Eng Sci*, 47, 1133 (2007).
8. Q.Guo, J. Wang, C.B. Park and M. Ohshima, *Ind Eng Chem Res*, 45, 6153 (2006).
9. S.N. Leung, C.B. Park, D. Xu, H. Li, R.G. Fenton, *Ind Eng Chem Res*, 45, 7823 (2006).
10. J.F. Palierne, *Rheol Acta*, 29, 204 (1990).
11. D. Graebing, R. Muller, and J.F. Palierne, *Macromol*, 26, 320 (1993).
12. Y. Otsuki and T. Kanai, *Polym Eng Sci*, 45, 1277 (2005).
13. G. Li, J. Wang, C.B. Park and R. Simha, *J Polym Sci: Polym Phys*, submitted February 2006.

14. S.G. Kim, C.B. Park and M. Sain, *SAE 2007 World Congress*, #07M-8, April 16-19 (2007).
15. K. Taki, K. Tabata, S. Kihara and M. Ohshima, *Polym Eng Sci*, 46, 680 (2006).
16. P. Rachtanapun, S.E.M. Selke and L.M. Matuana, *J App Polym Sci*, 93, 364 (2004).
17. P.C. Lee, J. Wang and C.B. Park, *Ind Eng Chem Res*, 45, 175, 2006.
18. C.Z. Sahagún, R. González-Núñez and D. Rodrigue, *J Cell Plast*, 42, 469 (2006).
19. K. Taki, K. Nitta, S.-I. Kihara and M. Ohshima, *J App Polym Sci*, 97, 189 (2005).

CHAPTER 5

Physical Properties and Foaming of Talc-Filled TPOs Based on Blends of Linear and Branched Polypropylene

5.1 Introduction

Polypropylene (PP) has proven to be a popular and effective material for use in numerous applications in a variety of industries. Recently, PP has shown much promise in the automotive industry for the production of foamed and thermoformed products due to its low cost and excellent processability. However, the use of PP in automotive parts is limited by its low melt strength, which somewhat limits its use in processes requiring excellent strain hardening behaviour. PPs with long-chain branching, which have recently become commercially available, exhibit higher melt strength, thereby improving foamability and thermoformability [1-4]. These materials offer new and exciting opportunities for PP blends which combine the properties of traditional linear PP with the high melt strength branched PP. However, the addition of branches in the PP melt may cause reductions in mechanical properties, such as the strain at break [5].

As shown in the previous chapter, the addition of various elastomers to PP blends of linear and branched PP has also proven to be effective in enhancing the applicability of PP by creating a blend with better impact strength and ductility at low temperatures, while lowering the tensile and flexural properties. The elastomeric components of these thermoplastic olefin (TPO) blends have traditionally been ethylene-propylene rubber (EPR) and ethylene-propylene-diene terpolymers (EPDM), however new improvements

in metallocene or single-site catalyzed ethylene- α -olefin technology offers new materials such as polyolefin elastomers (POEs). These impact copolymers with relatively low molecular weights and improved processibility compared with EPR are of great interest for use in impact modified low molecular weight PP [6]. However, the addition of the dispersed elastomer phase has a detrimental effect on the stiffness of the blend.

In an effort to improve the stiffness of TPOs, as well as improve their dimensional stability and lower the material costs, the addition of inorganic fillers offers considerable advantages and has widespread practice. Research into PP/elastomer blends containing various types of filler such as CaCO₃, talc and silica has been performed in the past [7-12]. Three types of microstructures for PP/elastomer/filler blends can be obtained depending on the location of the filler: the fillers may form a structure where the filler resides in the matrix, an encapsulation/core-shell structure where the filler preferentially partitions in the dispersed phase may be present, or a mixture of the two. Premphet *et al.* [10] studied the properties of PP/elastomer/CaCO₃ blends with EOR or EVA as the elastomer, and determined that the composites with separately dispersed elastomer and filler particles have a lower yield stress and higher modulus and impact strength than core-shell particles. Long *et al.* [11] used PP/elastomer blends with talc and CaCO₃ and found that the elastic modulus was higher when the filler and rubber particles were separated in the matrix, which is in agreement with Premphet *et al.*; however, they also reported an increase in impact strength when the rubber particles with filler core were distributed in the PP matrix.

It has been shown that the addition of talc to a PP system improves both the tensile and flexural modulus, as well as the impact strength and deflection temperature

under load; however these properties come at the expense of the ultimate tensile strength and elongation [13, 14]. Svehlova *et al.* studied the mechanical behaviour of TPO blends and determined that the effect of filler size depends on the type of PP in the blend [15]. In addition, Wong *et al.* found that filler size only affected impact strength, while filler coating impacted the flexural modulus, ultimate tensile strength and elongation [14].

This paper aims to characterize blends of linear and branched polypropylenes with ethylene- α -olefin elastomers and talc as filler, in an effort to make a useful material capable for injection foam molding applications. Given that as shown in the previous Chapter, there are no substantial benefits in using high amounts of branched PP, TPOs containing up to 40 wt% branched PP are investigated in this chapter.

5.2 Experimental

5.2.1 Materials

Two Basell (Elkton, MD) polypropylenes were used in this study. The first is a linear PP resin, Pro-fax PD702 (LPP) with an MFR (230°C/2.16kg, g/10min) of 35, and the second is a high melt strength branched PP resin, Pro-fax PF611 with an MFR of 30. Both materials have a density of 902 kg/m³.

The Dow Chemical Company (Midland, MI) is responsible for the metallocene-based ethylene- α -olefin copolymer used in this research. This ethylene-octene copolymer has a melt flow index (MFI) (190°C/2.16kg, g/10min) of 30 and a density of 870 kg/m³.

The uncalcinated talc, Jetfil 700c, was supplied by Luzenac (Greenwood Village, CO) and has a median particle size of 1.5 μ m and a maximum particle size of 10-12 μ m.

As outlined in the blend preparation section, a series of PP/POE samples (70/30 by weight) were prepared, with the PP matrix including a range of branched PP compositions (LPP/BPP 100/0, 80/20, 60/40 by weight). In addition, talc was added to these blends in a range of compositions (TPO/talc 100/0, 95/5, 90/10, 80/20 by weight).

5.2.2 Blend Preparation

All blend components were dry-blended with 0.2% antioxidant (Irganox B225 from CibaGeigy). The dry blended formulations were then compounded using a Haake Polylab Rheocord torque rheometer using a Haake Polylab Rheocord torque rheometer equipped with a Rheomix 610p mixing chamber and roller rotors as per Chapter 4.

5.2.3 Rheological Characterization

The viscoelastic properties of the blends were characterized in the shear oscillatory mode, using a controlled stress rheometer (ViscoTech by Rheologica) equipped with parallel plates 20 mm in diameter. The measurements were performed at a gap of 0.5 mm and a temperature of 180 °C, under nitrogen blanket. Samples used in the rheometer were compression molded discs approximately 2 mm in thickness and 25 mm in diameter and were prepared using a Carver hydraulic press, heated at 200°C.

5.2.4 Thermal Properties

To characterize the thermal properties of the blends, a TA Instrument Differential Scanning Calorimeter (DSC) Q1000 was used. Refer to Chapter 4 for the experimental procedure.

5.2.5 Scanning Electron Microscopy

To characterize the blend morphology, a JEOL JSM-840 scanning electron microscope was used. Using a freeze-fracturing technique, compression moulded samples prepared under liquid nitrogen, then etched in toluene for two hours. Prior to viewing under the microscope, the fracture surfaces were sputtered with gold.

5.2.6 Mechanical Properties

An Instron Universal Tester, model 3369, was used to determine the tensile and flexural properties of all the blends, and impact strength was tested using an Instron Izod impact testing apparatus, as previously outlined in Chapter 4.

5.2.7 Batch Foaming Experiments

Experiments were conducted using a batch foaming simulation system [16, 17]. The temperature and pressure in the simulation chamber were regulated using a thermostat and a syringe pump, respectively. An ADAC board was used to record the pressure drop during experimentation, while a high speed CCD camera was used to

record bubble behaviour. Sample preparation and details of the characterization are found in Chapter 4.

5.3 Results and Discussion

5.3.1 Rheological Characterization

One of the major drawbacks of adding fillers such as talc is that the viscosity of the composite increases dramatically, making it difficult to process. As seen in Figure 5.1, which summarizes the complex viscosities (η^*) and elastic moduli (G') for 70/30 PP/POE blends containing 20 wt% BPP and varying talc content, the addition of talc greatly increases the viscosity as well as the elastic modulus of the blends. The substantial increases are accompanied by yielding behaviour, which is typical of filled systems, especially those containing platelet-type fillers with high surface area [18].

On the contrary, the addition of a branched component has virtually no effect on the rheology of the system. In an effort to assess whether it will be possible for our formulations to be processed by injection moulding, a commercial TPO, containing 10-12 wt % talc, used already for this purpose is compared as a benchmark. As seen in Figure 5.1, the viscosity of our TPO formulations is well below the viscosity of the commercial TPO, suggesting excellent processability.

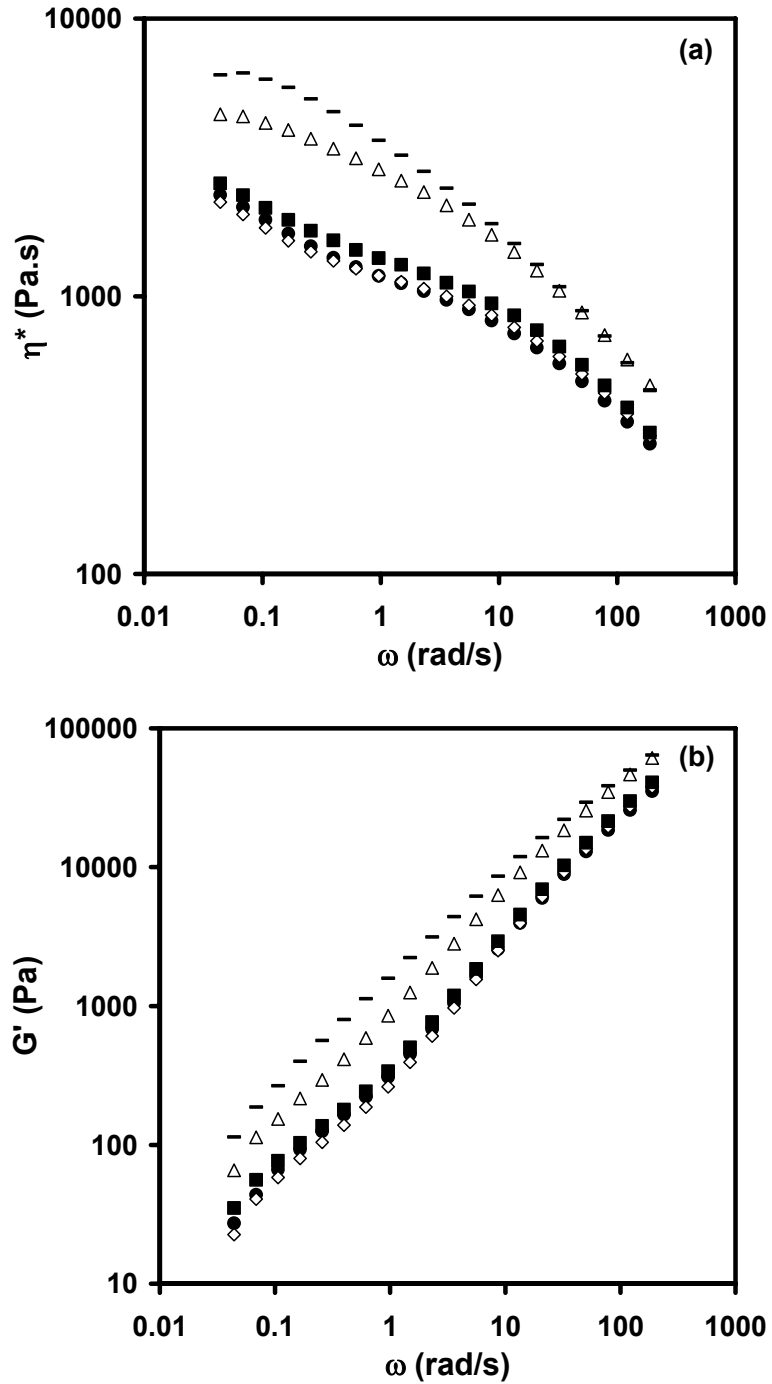


Figure 5.1. (a) Complex viscosities, η^* and (b) elastic moduli, G' , as a function of frequency, ω , for a commercial TPO resin (—) as well as for 70/30 PP/POE blends containing 20 wt% BPP and: ● 0 wt% talc, ◇ 5 wt% talc, ■ 10 wt% talc, △ 20 wt% talc.

5.3.2 Mechanical and Thermal Properties

The tensile properties of blends prepared with varying levels of branched PP, as well as talc, are represented in Figure 5.2. The addition of talc clearly increases the Young's modulus of the material, while decreasing the elongation at break. Therefore, these materials become stiffer with the addition of talc. As reported before [19], the addition of branched PP also has a negative effect on the toughness of the blends, however this effect is much less pronounced in the talc-containing composites.

Substantial gains in all flexural properties are realized when talc is added in the TPOs, as shown in Figure 5.3. The addition of branched PP has a minor effect on the flexural properties; the composites containing 20 wt% branched PP appear to be the most beneficial. The notched Izod impact tests performed show failures at -20°C of the composites containing 5 wt% talc with 0 or 20 wt% BPP, with impact energies of 0.0108 and 0.0132 J/m², respectively. None of the samples failed at room temperature.

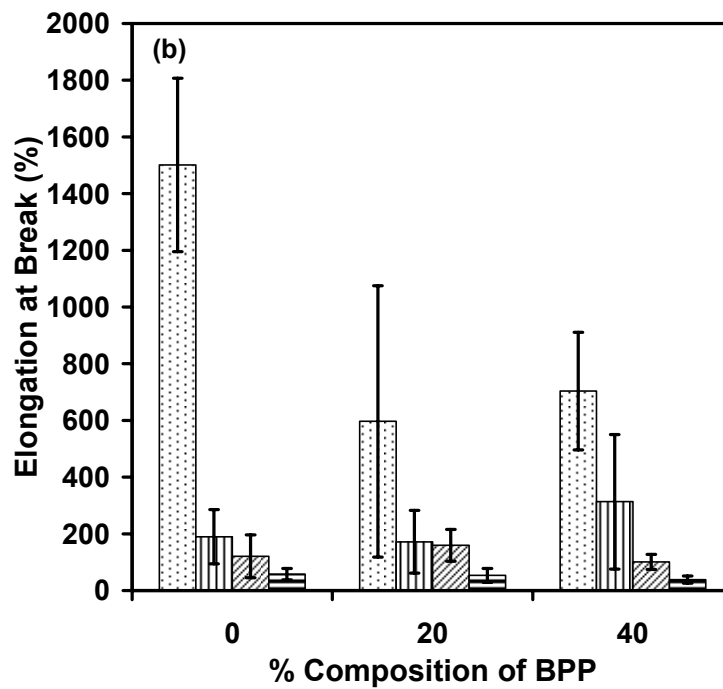
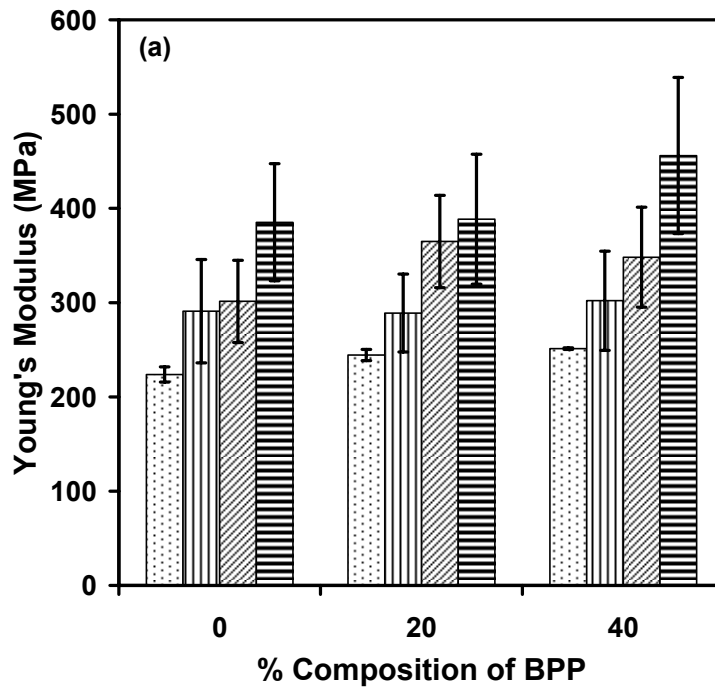
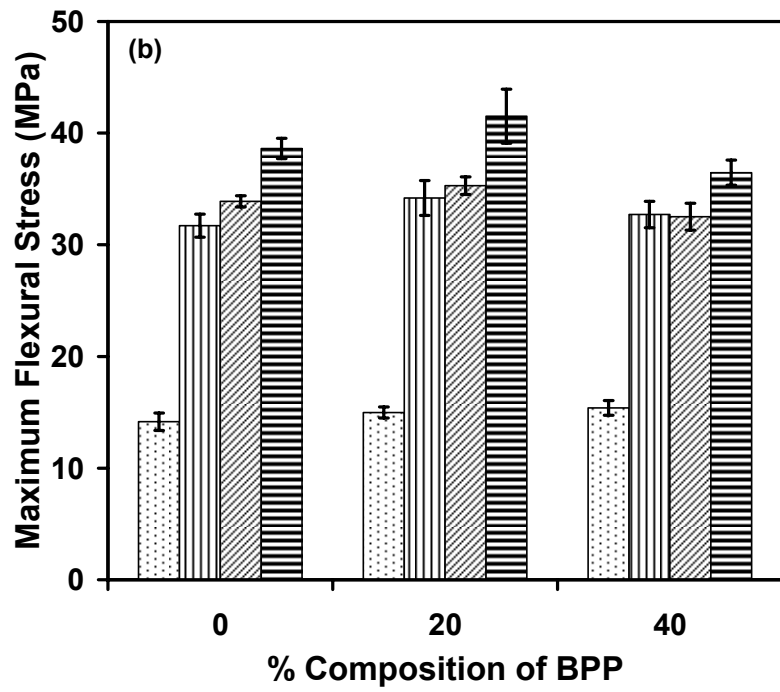
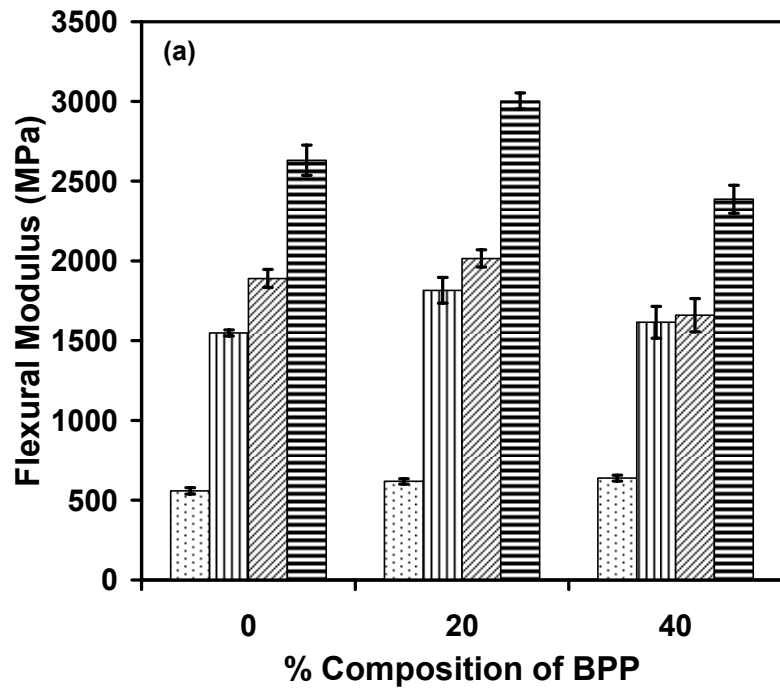


Figure 5.2. (a) Young's moduli and (b) elongation at break as a function of BPP content; 0 wt% talc, 5 wt% talc, 10 wt% talc, 20 wt% talc. Error bars represent 95% confidence intervals.



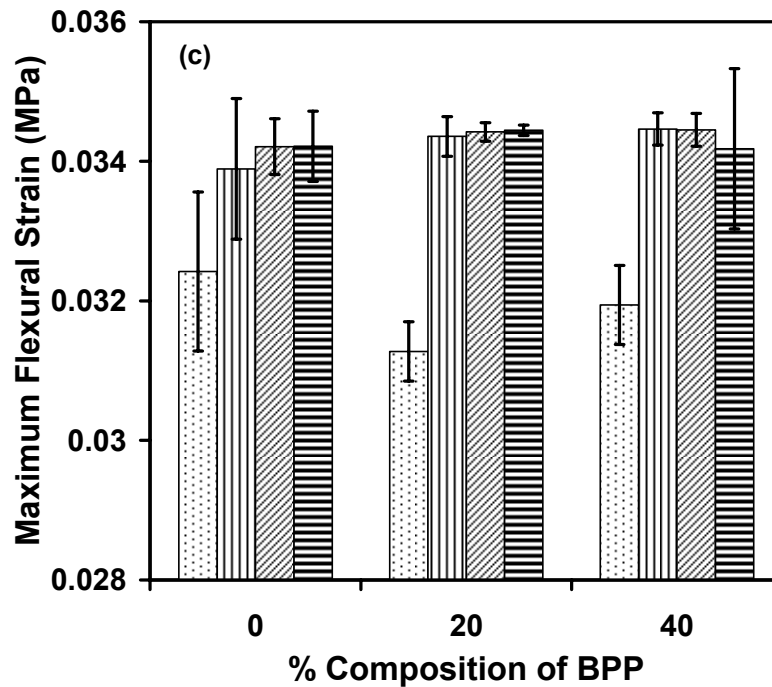


Figure 5.3. (a) Flexural moduli, (b) flexural stresses and (c) flexural strains as a function of BPP content; 0 wt% talc, 5 wt% talc, 10 wt% talc, 20 wt% talc. Error bars represent 95% confidence intervals.

The gains seen in stiffness and flexural properties are associated to the increases in crystallinity in the presence of talc. As shown in Table 5.1, addition of talc results in a higher heat of fusion, which translates to higher crystallinity. It is well known that talc acts as a nucleating agent for the crystallization of the PP spherulites [20], causing a shift in the crystallization temperature, as shown in Table 5.1. The shift is more pronounced for the blends containing only linear PP, this is why these blends benefited most from the addition of talc.

Talc particles also appear to have a slight nucleating effect on the elastomer phase, as shown in Figure 5.4 and Table 5.1. This finding suggests that the talc particles reside both in the PP and POE phases. SEM images (Figure 5.5) do indeed show that the

talc particles, with typical sizes ranging from 2.5 to 10 μm , are in contact with both phases. The fact that talc particles affect the elastomeric phase, in addition to the PP phase, is a drawback in the conventional practice of adding talc to these TPO composites, because in the presence of the filler the elastomeric phase may lose some of its inherent toughness. Approaches that aim at creating a separated microstructure, where the filler resides in the matrix phase alone are therefore much more desirable.

Table 5.1. Thermal properties of compounded TPOs (both with and without 10 wt% talc) containing varying levels of Branched PP.

BPP matrix content (wt. %)	T_c (PP matrix)	T_c (POE)	T_m	Heat of Fusion (J/g)
<i>TPO</i>				
0%	118.49	47.56	156.40	50.93
20%	126.09	49.80	158.15	54.48
40%	126.64	48.25	157.89	51.40
<i>TPO with 10 wt% talc</i>				
0%	127.82	47.58	159.33	55.07
20%	128.74	47.37	158.81	56.08
40%	129.92	47.58	158.45	55.58

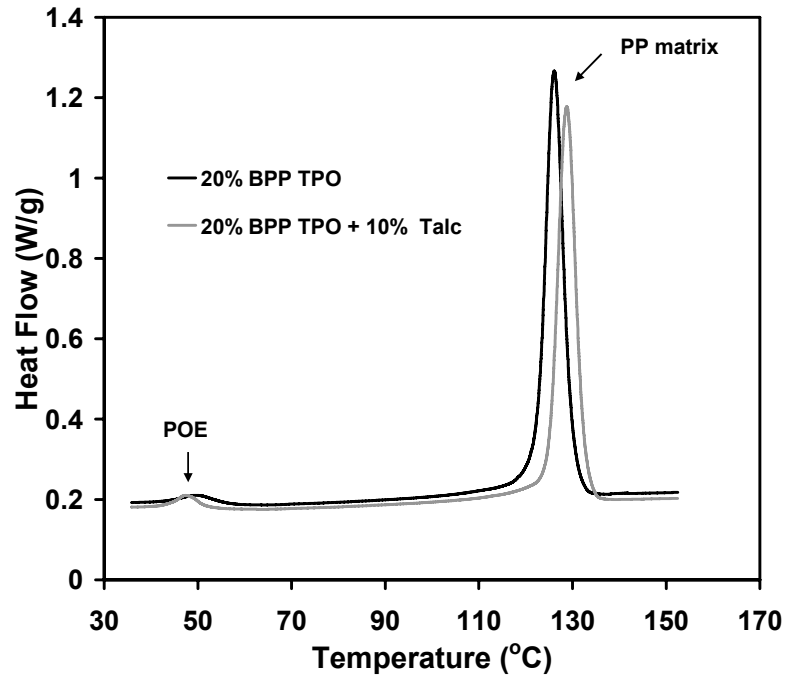
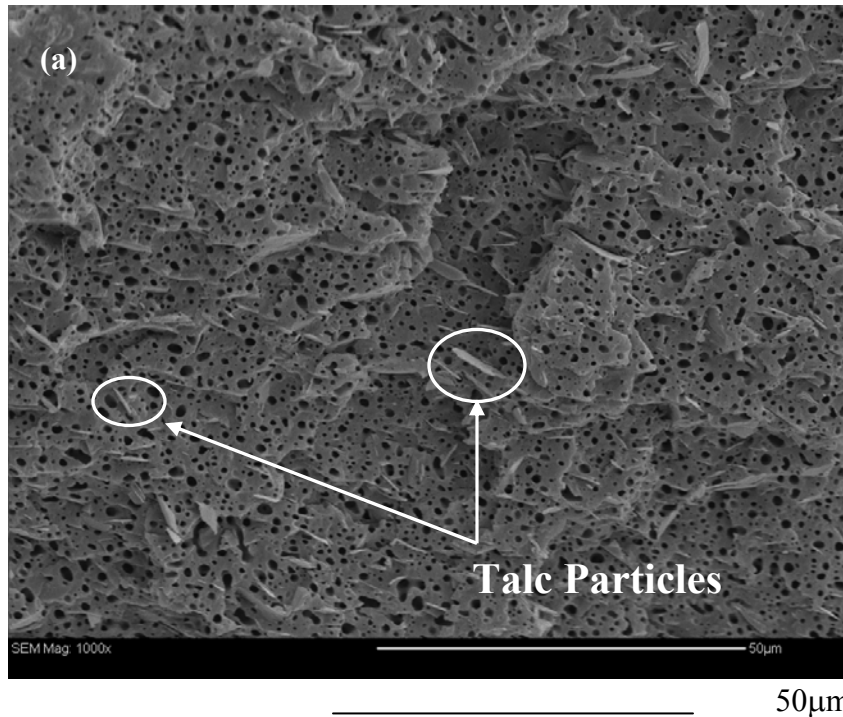


Figure 5.4. Cooling curve showing T_c for blends containing 20% branched PP both with and without 10 wt% talc.



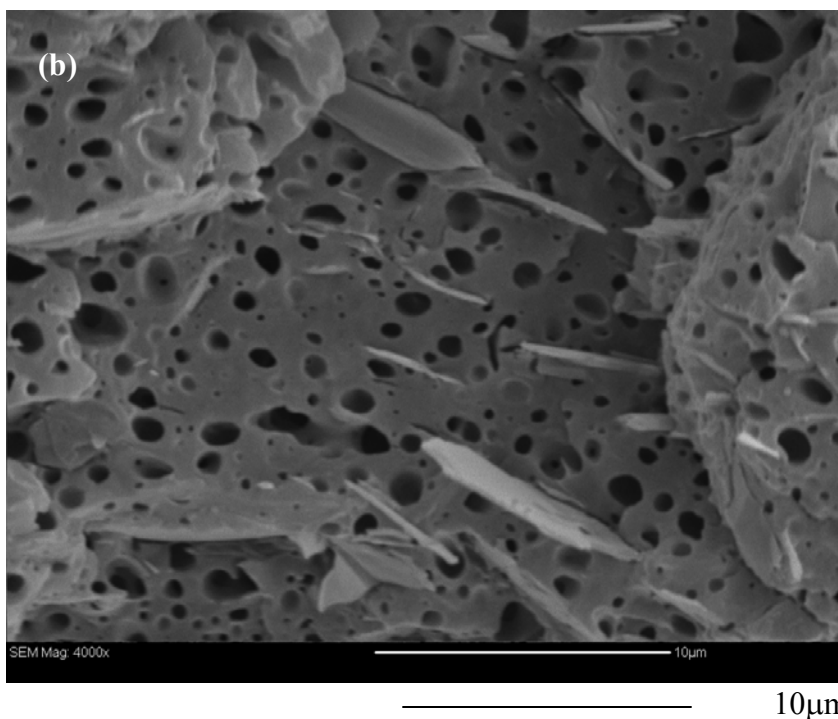


Figure 5.5. SEM images at (a) 1000x magnification and (b) 4000x magnification of 70/30 LPP/elastomer with 10 wt% talc.

5.3.3 *Batch Foaming Experiments*

Figure 5.6 shows the cell densities obtained from foaming simulations for the PP/POE blends containing 10 wt % talc and varying amounts of branched PP. Given that the standard deviation in these experiments was in the order of $\pm 6 \cdot 10^6$ cells/cm³, the difference between the foamed samples when the content of branched PP is increased is negligible. As noted before in Chapter 4, there is a trend towards decreased cell growth rates and cell density when adding branched PP. The corresponding maximum cell densities, shown in Figure 5.7, also reflect the same trend. Therefore for these composites, the addition of branched PP does not seem to have any beneficial effect on the growth rates and any benefits should come from the prevention of cell coalescence, which should be the subject of future investigation.

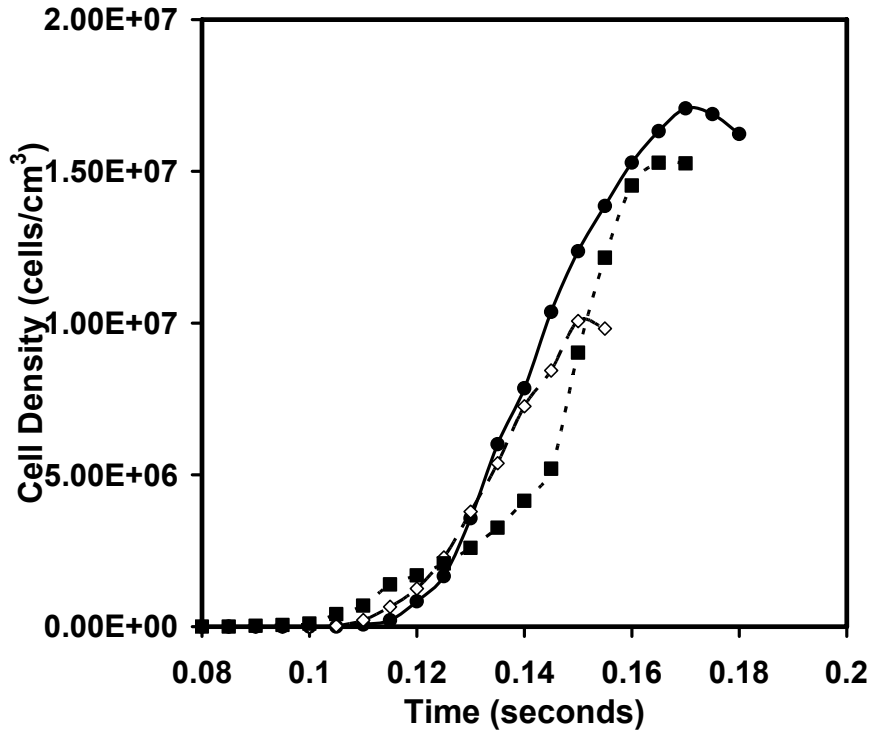


Figure 5.6. Cell densities as a function of time for foamed 70/30 PP/POE blends containing 10 wt % talc and: ● 0 wt% BPP, ◇ 20 wt% BPP, ■ 40 wt% BPP.

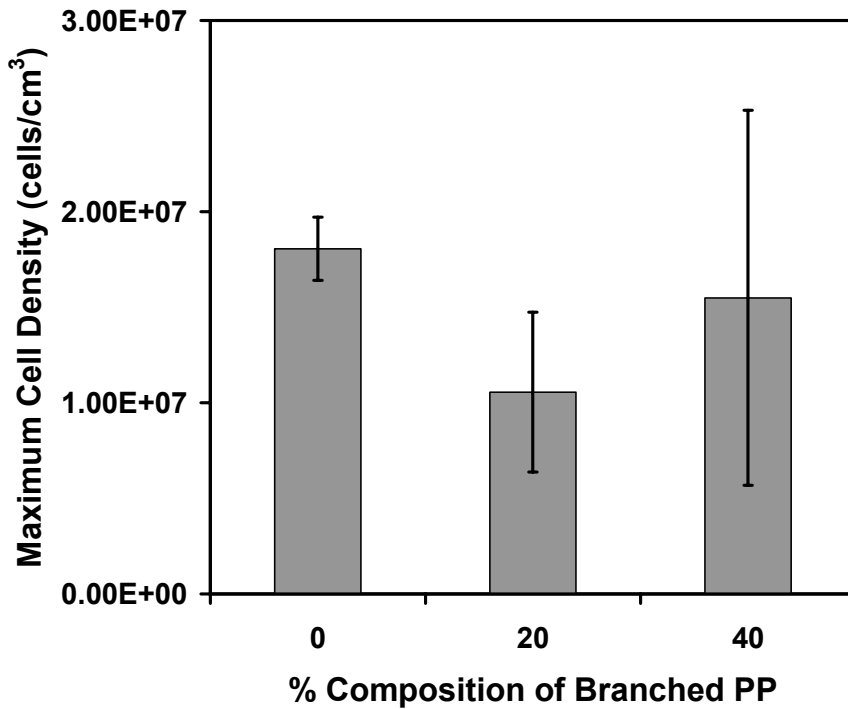


Figure 5.7. Maximum cell density as a function of BPP content for the TPO blends with 10 wt% talc.

5.4 Conclusions

The addition of talc to TPO blends increases the viscosity and elastic modulus and affects the thermal properties of the blends. Increases in the crystallinity of the talc-filled samples are the cause of the gains in the stiffness and flexural properties of the blends. Optimum gains were realized in the TPOs containing 20 wt% branched PP. Foaming studies showed that increasing levels of branched PP did not substantially affect the bubble growth rate or the final cell density.

5.5 References

1. G.J. Nam, J.H. Yoo and J.W. Lee, *J App Polym Sci*, 96, 1793 (2005).
2. P. Spitael and C.W. Macosko, *Polym Eng Sci*, 44, 2090 (2004).
3. H.E. Naguib, J.X. Xu, C.B. Park, A. Hesse, U. Panzer, and N. Reichelt, *Proceedings SPE ANTEC*, 2, 1623 (2001).
4. H.E. Naguib, C.B. Park, A. Hesse, and U. Panzer, *Polym Eng Sci*, 42, 1481 (2002).
5. A.D. Gotsis and B.L.F. Zeevenhoven, *Polym Eng Sci*, 44, 973 (2004).
6. M. Kontopoulou, W. Wang, T.G. Gopakumar, and C. Cheung, *Polymer*, 44, 7495 (2003)
7. R. Uotila, U. Hippel, S. Paavola and J. Seppala, *Polymer*, 46, 7923 (2005).
8. X. Su, Y. Hua, J. Qiao, Y. Liu, X. Zhang, J. Gao, et al., *Macromol Mater Eng*, 289, 275-280 (2004).
9. J. Jancar and A.T. Dibenedetto, *J Mater Sci*, 30, 1601 (1995).
10. K. Premphet and P. Horanont, *J Appl Polym Sci*, 76, 1929 (2000).
11. Y. Long and R.A. Shanks, *J Appl Polym Sci*, 61, 1877 (1996)
12. Y. Long and R.A. Shanks, *J Appl Polym Sci*, 62, 639 (1996).

13. P. Gaskell and A.C.Smith, *Plastics, Rubber and Composites Processing and Application*, 22, 171 (1994).
14. T.L. Wong, C.M.F. Barry and S.A. Orroth, *Proceedings SPE ANTEC* (1995).
15. V. Svehlova and E. Poloucek, *Angew Makromol Chem*, 214, 91 (1994).
16. Q. Guo, J. Wang, C.B. Park and M. Ohshima, *Proceedings SPE ANTEC*, 2, 2615 (2004).
17. S.N. Leung, C.B. Park, D. Xu, H. Li, R.G. Fenton, *Ind Eng Chem Res*, 45, 7823 (2006).
18. S.A. Khan and R.K. Prud'homme, *Reviews in Chem Eng*, 4, 205 (1987).
19. T.J. McCallum, M. Kontopoulou, C.B. Park, E.B. Muliawan, and S.G. Hatzikiriakos, *Polym Eng Sci*, 47, 1133 (2007).
20. B. Pukanszky and J. Moczo, *Macromol Symp*, 214, 115 (2004).

CHAPTER 6

Conclusions and Recommendations

6.1 Conclusions

Blends of linear and branched PPs exhibited increased melt elasticity and strain hardening, and produced more pronounced shear thinning behaviour. Based on the rheological and thermal characterization, these blends appeared to be miscible.

The melting points and crystallinities were affected substantially upon introduction of the higher molecular weight BPP2.5 resin, whereas they remained virtually unaffected in the presence of BPP30. The crystallization points increased significantly upon addition of low amounts of branched PPs for both sets of blends.

The flexural properties and tensile moduli increased with the introduction of branched PP; the blends containing BPP30 displayed better mechanical properties; this was credited to the higher crystallinity of BPP30.

Addition of branched PP in TPOs does not alter significantly the morphology or the interfacial tension between the blend components, although some coarsening is seen at high POE contents, possibly due to an increase in the coalescence rate in the presence of a more elastic matrix.

All materials containing branched PP are generally more rigid and have enhanced flexural properties, accredited to the increase in the blend crystallinity. However, these qualities come at the expense of the elongation at break, although even at low temperatures, all blends show good toughness.

Foaming experiments performed using a batch foaming simulation apparatus indicated that the addition of branched PP did not affect substantially the rate of bubble growth in the TPOs and blends containing amounts of 40-80% branched PP showed slower cell growth rates and decreased cell densities.

The addition of talc to TPO blends increases the viscosity and elastic modulus and affects the thermal properties of the blends. Increases in the crystallinity of the talc-filled samples are the cause of the gains in the stiffness and flexural properties of the blends. Optimum gains were realized in the TPOs containing 20 wt% branched PP. Foaming studies showed that increasing levels of branched PP did not substantially affect the bubble growth rate or the final cell density.

6.2 Recommendations for Future Work

1. A detailed characterization of the solubility of the nitrogen blowing agent into the various TPO formulations is needed, in order to provide further in depth interpretation of the foaming results.
2. Based on our results using branched PP did not generally have a positive effect on the foaming process. However, the experiments performed in the batch foaming apparatus cannot show the coarsening of the foam structures, which is where most of the benefits are expected to occur. Carefully designed experiments, possibly by extrusion or injection foam molding experiments are needed in order to carefully characterize the effect of the branched material on the cell coalescence process.

3. It would be of interest to characterize the mechanical properties of the final foamed structure, to verify whether the characteristics of the unfoamed plastics persist when they are foamed.